

**RESEARCH ARTICLE**

# Open Source Variational Quantum Eigensolver Extension of the Quantum Learning Machine (QLM) for Quantum Chemistry

Mohammad Haidar\*<sup>1,2,3</sup> | Marko J. Rančić<sup>3</sup> | Thomas Ayral<sup>4</sup> | Yvon Maday<sup>2,5</sup> | Jean-Philip Piquemal\*<sup>1</sup>

arXiv:2206.08798v2 [quant-ph] 22 Jun 2022

<sup>1</sup>Sorbonne Université, Laboratoire de Chimie Théorique(UMR-7616-CNRS), 4 place Jussieu-75005 Paris, France

<sup>2</sup>Sorbonne Université, CNRS, Université Paris Cité, Laboratoire Jacques Louis Lions (LJLL), 4 place Jussieu-75005 Paris, France

<sup>3</sup>TotalEnergies, Tour Coupole La Défense, 2 Pl. Jean Millier, 92078 Paris, France

<sup>4</sup>Atos Quantum Laboratory, Les Clayes-sous-Bois, France

<sup>5</sup>Institut Universitaire de France, Paris, France

**Correspondence**

Mohammad Haidar, Sorbonne Université, Laboratoire de Chimie Théorique(UMR-7616-CNRS) and Laboratoire Jacques Louis Lions (UMR-7598-CNRS), 4 place Jussieu, 75005 Paris, France. Email:

mohammad.haidar@upmc.fr;

Marko J. Rančić, Tour Coupole La Défense, 2 Pl. Jean Millier, 92078 Paris, France.

Email: marko.rancic@totalenergies.com;

Jean-Philip Piquemal, Sorbonne Université, Laboratoire de Chimie Théorique(UMR-7616-CNRS). Email: jean-philip.piquemal@sorbonne-universite.fr

## Abstract

Quantum Chemistry (QC) is one of the most promising applications of Quantum Computing. However, present quantum processing units (QPUs) are still subject to large errors. Therefore, noisy intermediate-scale quantum (NISQ) hardware is limited in terms of qubits counts and circuit depths. Specific algorithms such as Variational Quantum Eigensolvers (VQEs) can potentially overcome such issues. We introduce here a novel open-source QC package, denoted Open-VQE, providing tools for using and developing chemically-inspired adaptive methods derived from Unitary Coupled Cluster (UCC). It facilitates the development and testing of VQE algorithms. It is able to use the Atos Quantum Learning Machine (QLM), a general quantum programming framework enabling to write, optimize and simulate quantum computing programs. Along with Open-VQE, we introduce myQLM-fermion, a new open-source module (that includes the key QLM resources which are important for QC developments (fermionic second quantization tools etc..)). The Open-VQE package extends therefore QLM to QC providing: (i) the functions to generate the different types of excitations beyond the commonly used UCCSD ansatz; (ii) a new implementation of the "adaptive derivative assembled pseudo-Trotter method" (ADAPT-VQE), written in simple class structure python codes. Interoperability with other major quantum programming frameworks is ensured, thanks to myQLM, which allows users to easily build their own code and execute it on existing QPUs such as IBM, Google, Rigetti or Microsoft, etc... The combined Open-VQE/myQLM-fermion quantum simulator facilitates the implementation, tests and developments of variational quantum algorithms towards choosing the best compromise to run QC computations on present quantum computers while offering the possibility to test large molecules. We provide extensive benchmarks for several molecules associated to qubit counts ranging from 4 up to 24 where we focus our work on reaching chemical accuracy, reducing the number of circuit gates and optimizing parameters and operators between "fixed-length" UCC and ADAPT-VQE ansatze.

**KEYWORDS:**

Quantum chemistry, Open-VQE, Quantum Learning Machine, myQLM-fermion, Variational Quantum Eigensolvers, unitary coupled cluster family, ADAPT-VQE.

## 1 | INTRODUCTION

Solving the Schrödinger equation to obtain the many-electron wavefunction is the central problem of modern quantum chemistry<sup>1,2</sup>. In practice, it is possible to achieve full accuracy for systems that contain few electrons through methods like the Full Configuration Interaction (FCI) and the Full Coupled-Cluster (FCC), which include all the electron configurations. However, the computational cost grows exponentially when the number of electrons increases, as the dimension of the FCI and FCC wave functions. For example, the number of possible Slater determinants increases as a function of the number of electrons  $n_e$  and of orbitals  $n_o$ <sup>3</sup>:

$$\dim \mathcal{H} \approx (n_o! / [(n_o - n_e/2)!(n_e/2)!])^2. \quad (1)$$

Attempts to reach full accuracy on large systems clearly faces the so-called “exponential wall” that limits the applicability of the most accurate methods to more complex chemical systems. So far, the largest calculations performed with classical supercomputers have only included tens of billions of determinants (see<sup>4</sup>) with (20 electrons, 20 orbitals) with hopes to solve problems of a size close to a trillion determinants (24 electrons, 24 orbitals) in a near future thanks to the advances of massively parallel supercomputer architectures.<sup>5</sup> Given such constraints, other classes of methods have to be used to approximate the ground state wavefunctions for larger many electrons systems. They include: (i) Density-Functional Theory (DFT), which relies on the use of a single Slater determinant, and has been shown to be extremely successful while failing to describe strongly correlated systems<sup>6,7,8</sup>; (ii) post Hartree-Fock methodologies such as the truncated Coupled-Cluster (CC) and the Configuration Interaction (CI) approaches that, even though being still operational beyond the single Slater determinant, cannot be applied to large size molecules, due to their extreme computational requirements in terms of Slater determinants<sup>9,10,11,12,13,14,15,16</sup>. A good example is provided by the “gold standard” methods denoted coupled-cluster single-, double-, plus perturbative triple-excitations CCSD(T). Indeed, CCSD(T) is able to handle a few thousands basis functions, but at the cost of an enormous operation counts that is limited by the large requirements in term of data storage.<sup>17</sup> No matter the choice of chemical basis sets (STO-3G, 6-31G, cc-pVDZ, and beyond...), these methods are insufficient to reach accurate enough results for large molecules.

A paradigm shift proposed by Feynman<sup>18,19</sup> is to use quantum computers for simulating quantum systems. This has prompted the community to use quantum computers in order to solve the quantum chemistry wavefunction problems. Intuitively, the advantage comes from the fact that quantum computers can process “exponentially” more information than classical computers<sup>20</sup>. Recent reviews provide a background about strategies for developing quantum algorithms dedicated to Quantum Chemistry. These approaches include techniques such as Quantum Phase Estimation (QPE), Variational Quantum Eigensolvers (VQEs) or quantum Imaginary Time Evolution (QITE).<sup>21,22,23,24</sup> All methods generally include three key steps: (i) transforming the wavefunction into qubits; (ii) constructing circuits with one and two-qubit quantum gates; (iii) using the circuits to measure the expectation value of a given Hamiltonian. However, currently, available quantum computers remain in the Noisy Intermediate-Scale Quantum (NISQ) era and are limited by two main resources: the number of qubits and the circuit depth (i.e. number of quantum gates)<sup>25,26,27,28</sup>. Among all available strategies, the VQE family of techniques is a very promising algorithm that can be applied to NISQ hardware<sup>21,29,30,21,31</sup>. Indeed, it is better suited to such devices than other algorithms such as QPE, thanks to its more modest requirements in term of quantum processor coherence times and it has already been successfully executed on real NISQ quantum computers based on various technologies including superconducting qubits<sup>32,33</sup>, photons<sup>29</sup> and trapped ions<sup>34</sup>. It is known that the performance of VQE algorithms is highly dependent on the type of wavefunction ansatz. In practice, several types of ansatze can be used including: unitary coupled-cluster (UCC) wavefunctions<sup>35,36</sup>, hardware-efficient<sup>33,37</sup>, qubit coupled cluster (QCC)<sup>38</sup>, deep multi-scale entanglement renormalization ansatz (DMERA)<sup>39</sup> and Hamiltonian variational<sup>40</sup>. Furthermore, there are recent hybrid approaches such as adaptive ansatz<sup>41</sup> and subspace expansion method<sup>42</sup>, that also utilize the basic VQE scheme to build the wavefunction of the system.

In this article, we provide a newly-designed software package named "Open-VQE" that extends the Atos Quantum Learning Machine ("QLM"). QLM is a quantum computing platform that allows to write hardware-agnostic quantum programs, compile them in compliance with hardware constraints, and either emulate them classically with realistic noise or execute them on actual quantum hardware. QLM is a mix between commercial tools and non-commercial ones provided by the Atos company. Open-VQE is fully compatible with the freely available (open source) component of QLM called "myQLM", which is available online<sup>43</sup>. myQLM is a quantum software stack for writing, simulating, optimizing, and executing quantum programs. It provides within a python interface: (i) a powerful semantics for manipulating quantum circuits, with support for universal as well as custom gate sets, abstract parameters, advanced linking options, etc; (ii) a versatile execution stack for running quantum jobs, including an easy handling of observables, special plugins for carrying out NISQ-oriented variational methods (such as VQE

or QPE), and easy application programming interface for writing customized plugins (e.g., for compilation or error mitigation), as well as for connecting to any Quantum Processing Unit (QPU); (iii) a seamless interface to available quantum processors and major quantum programming frameworks<sup>44</sup>. The capacity of QLM/myQLM to interoperate with other packages such Qiskit<sup>45</sup>, Cirq<sup>46</sup> and PyQuil<sup>47</sup> etc, allows researchers from different horizons to communicate, interact, exchange, and work more efficiently and faster. Furthermore, myQLM acts as an intermediate for users who want to access quantum computers (IBM, Google etc...), providing them simple keys to run directly their jobs. myQLM comes with fermionic second quantization tools, which are helpful for solving quantum chemistry problems. These tools are now included in a new specialized open source module called "myQLM-fermion" that is part of the present work and designed to work synergistically with Open-VQE. It includes the key QLM resources that are important for Quantum Chemistry developments. In particular, we use two important tools provided by myQLM-fermion which are useful for quantum resource reductions<sup>35</sup>: (i) an active space (AS) selection approach that is useful for the reduction of the number of qubits; (ii) MP2 pre-screening approach that involves an implementation of second order Møller-Plesset perturbation (MP2) amplitudes as an input guess that is useful for faster parameter optimization. By using the initial myQLM building blocks, we were able to design our Open-VQE package, which provides the community with advanced VQE tools especially dedicated to quantum chemistry problems needed to be solved by quantum computers. Open-VQE mainly includes simple modules dedicated to the UCC family and to adaptive ansatze algorithms. These modules comprise various features including:

1. different types of UCC generators (truncated to single and double excitations): (i) Unitary Coupled Cluster Singles and Doubles (UCCSD<sup>48</sup>) approaches; (ii) Unitary Pair CC with Generalized Singles and Doubles Product (k-UpCCGSD<sup>49</sup>) techniques; (iii) the possibility of including excitations that form spin-complemented pair interactions<sup>41</sup> and excitations that conserve only singlet spin symmetry of UCCGSD (see appendix of<sup>50</sup>); (iv) Qubit Unitary Coupled Cluster Singles and Doubles QUCCSD<sup>51</sup>;
2. adaptive VQE algorithms (namely Adaptive Derivative-Assembled Pseudo-Trotter-VQE (ADAPT-VQE)), with different operator pools including: (i) Unitary fermionic operators (fermionic ADAPT-VQE<sup>41</sup>); (ii) Anti-Hermitian Pauli operators (qubit ADAPT-VQE<sup>50,52</sup>).

These modules are structured in simple python classes requiring to write only a few lines of code. Furthermore, they provide examples for the facile and rapid implementation of additional algorithms on the basis of myQLM basic tools.

The goal of the paper is to showcase the novel Open-VQE/myQLM-fermion combined quantum simulator package that enables researchers to test, develop and measure the computational requirements of VQE flavors towards their future potential implementation on real supercomputers. It allows to compare the accuracy of the total molecular energies obtained thanks to various variants of the UCC method to popular quantum chemistry methods using classical computers. The GitHub websites of Open-VQE<sup>53</sup> and myQLM-Fermion<sup>54</sup> are public, under "MIT" and "Apache-2.0" licenses, respectively.

The paper is organized as follows: we review the theory of UCC ansatze including the different types of excitations, the ADAPT-VQE approach and the different steps needed to implement it (section 2). We then introduce the QLM library, specifically its myQLM-fermion open source extension while focusing for the first time on the quantum chemistry tools that can help us to develop Open-VQE (see section 3). We then describe Open-VQE and its several implementations of the UCC and ADAPT-VQE families of methods and show how myQLM-fermion components can be used to develop those modules through simple codes (section4). Finally, applying Open-VQE to our in-house HPC architecture (QLM simulator server at Total energies), we simulate a full set of molecules ranging from 4 to 24 qubits. We first show the properties of the simulator applied to a set of small molecules. Second, we describe how Open-VQE/myQLM-fermion can use the active space selections and MP2 pre-screening initial guesses through computations on different test molecules. Then using the UCC methods module we compare the UCCSD to QUCCSD ansatz in terms of quantum gates, and then compare the chemical accuracy achieved by these algorithms to those obtained by robust computational methods using classical computers. Afterwards, using our ADAPT-VQE module we compare the fermionic and qubit ADAPT-VQE results obtained on a set of molecules in terms of chemical accuracy, numbers of variational parameters, operators and quantum gates. We detail a specific analysis for each of the fermionic and qubit ADAPT-VQE. Finally, we compare the group of "fixed-length" ansatze to the ADAPT-VQE (section5). We conclude with a Table comparing the features of the Open-VQE/myQLM-fermion packages with those implemented in other software packages, while giving some perspectives towards the development of new types of UCC ansatze and/or new variational algorithms within Open-VQE in order to efficiently solve quantum chemistry problems.

## 2 | REVIEW: UNITARY COUPLED CLUSTER (UCC) AND ADAPTIVE DERIVATIVE-ASSEMBLED PSEUDO-TROTTER (ADAPT) WITHIN THE VQE ALGORITHM

We will use the following notations in the article: the indices  $i$  and  $j$  refer to the occupied spin-orbitals in the Hartree-Fock (HF) state; indices  $a$  and  $b$  refer to the unoccupied (or virtual) spin-orbitals in the HF state. Indices  $p, q, r$  and  $s$  are always related to spin-orbitals unless mentioned otherwise. When the orbitals are associated to an  $\alpha$ -like symbol ( $p_\alpha, q_\alpha, \dots$ ) they refer to spin-up electrons, and those with a  $\beta$ -like symbol ( $p_\beta, q_\beta, \dots$ ) refer to spin-down electrons.  $n_e$  and  $n_o$  (as given in the introduction) represent the number of electrons and orbitals, respectively. We also denote  $\eta$  and  $N_A$  by the number of active electrons and number of active spin-orbitals, respectively, and by  $n$  the number of qubits. In qubit representation we assign  $|\psi_{ref}\rangle$  by the  $n$ -qubit initial state transformation represented by a ket-state  $|q_0, q_1, q_2, q_3, \dots, q_n\rangle$ . We call  $|\psi(\theta)\rangle$  the trial wave function and  $\theta$  its variational parameter,  $U(\theta)$  a parameterized unitary operator.

### 2.1 | Variational Quantum Eigensolver (VQE)

The Variational Quantum Eigensolver (or VQE) has been first developed by Peruzzo et al.<sup>29</sup> and has received significant attention from the research community in recent years. It aims at finding the ground state energy  $E_0$  of a given Hamiltonian  $H$  either in quantum chemistry, condensed matter, or nuclear physics. In our work and since we mainly focus on the quantum chemistry problems, our Hamiltonian model is written in the fermionic second quantization form as:

$$H = \sum_{pq} h_{pq} c_p^\dagger c_q + \frac{1}{2} \sum_{pqrs} h_{pqrs} c_p^\dagger c_q^\dagger c_r c_s, \quad (2)$$

where  $c_p^\dagger (c_q)$  are anti-commuting operators that create (annihilate) electrons in spin-orbital  $p (q)$ , respectively. The symbols  $h_{pq}$  and  $h_{pqrs}$  denote the one- and two-body integrals of the corresponding operators and spin-orbitals in Dirac notation, respectively. These integrals can be easily computed on a classical computer.

The VQE method is based on quantum variational theory, whose starting point is the Rayleigh-Ritz variational principle, which states that

$$\langle \psi(\theta) | H | \psi(\theta) \rangle \geq E_0, \quad (3)$$

namely the energy of the normalized “trial” function  $|\psi(\theta)\rangle$  provides an upper bound for the ground state energy  $E_0$ . An iterative process minimizes the expectation value  $E(\theta) = \langle \psi(\theta) | H | \psi(\theta) \rangle$  with respect to the parameterized trial state  $|\psi(\theta)\rangle$ , that, eventually, converges and gives an approximation of  $E_0$  at the end of the process.

VQE is an hybrid classical-quantum implementation of the above variational iterative method that benefits from using both classical and quantum computers. It uses the quantum computer for the state preparation and energy measurement evaluations which are the costly part in the VQE process, and the classical computer for performing the optimization required to update the quantum state of the system. In order to see how this process works, we outline below the steps needed to perform a single iteration of the VQE algorithm (see for example Figure 1 in<sup>29</sup>):

1. Preparation of the trial state  $|\psi(\theta)\rangle$  on the quantum computer (or Quantum Processing Unit, QPU) with a circuit which includes a set of one- and two-qubit parameterized gates (or even multi-qubit gates used for example for trapped ion case<sup>55</sup>).
2. Once the circuit is prepared, the energy of the Hamiltonian given in Eq. 2 is measured. This is done by transforming it from a fermionic to a qubit representation (using e.g., the Jordan Wigner (JW) transformation<sup>56</sup>). This allows to express it as a sum of Pauli strings (i.e. tensor products of Pauli operators):

$$H = \sum_j h_j P_j, \quad (4)$$

with  $P_j = \prod_{i=0}^{n_o-1} \sigma_i^j$ , where  $\sigma_i$  is a Pauli matrix involving qubit  $i$ . Once the Hamiltonian is written in this basis, the energy is computed by measuring the expectation value of each Pauli string over the qubit representation of the circuit, and summing over the measurements. The results of multiple measurements are then averaged to obtain the energy

$$E(\theta) = \sum_j h_j \langle \psi(\theta) | \prod_{i=0}^{n_o-1} \sigma_i^j | \psi(\theta) \rangle. \quad (5)$$

3. The energy and qubit rotation parameters are then fed into a classical computer that runs an optimisation algorithm (e.g., COBYLA, SLSQP or BFGS)<sup>57</sup>, which returns a new set of parameters. In order to reach convergence faster, initial guesses of ansatz parameters of cluster operators obtained from the second-order Møller-Plesset perturbation theory can be used.<sup>35</sup>

4. The new set of parameters then used to prepare a new parametrized circuit from which a new sum over Pauli strings expectation values, and hence a new energy expectation value, is calculated.

5. The previous two steps are repeated until a convergence criterion, typically the difference in energy between VQE iterations, is below some threshold value, controlled by the conditions of the chosen optimizer method. To get more information about VQE, the interested reader could refer to a detailed analysis of the algorithm by Cao et al.<sup>22</sup> and to a review detailing its application to quantum chemistry<sup>21</sup>. An overview of VQE efficiency using NISQ devices has also been recently proposed by Bharti et al.<sup>28</sup>.

## 2.2 | Unitary Coupled Cluster (UCC) approach within VQE

The degree of accuracy with which VQE obtains an approximate minimum energy of an electronic structure Hamiltonian with a very good approximation of the ground state depends on several keys features such as the choice of the quantum state prepared on a quantum device (circuit), the iterative solver, the number of iterations, the number of CC excited levels.

The unitary coupled cluster (UCC) approach, which is inspired from the classical coupled cluster computational method<sup>58,59,9,15</sup>, has been shown to be a good choice for reaching accurate results. It was originally introduced to the area of quantum chemistry computations<sup>14</sup> and was later successfully implemented using quantum computers<sup>60,29</sup> thanks to its inherent simplicity. A comprehensive review of the UCC method is given in<sup>35,36</sup>. UCC yields variational states prepared by using unitary evolution under a sum of fermionic terms associated with their variational parameters. These terms represent the fermionic excitations that occur on the top of the initial Hartree Fock (HF) state. The UCC wavefunction can be then expressed as follows:

$$|\psi_{UCC}\rangle = e^{T-T^\dagger} |\psi_{HF}\rangle \quad (6)$$

where  $T$  is the cluster operator and  $T^\dagger$  is its Hermitian conjugate. As  $T$  is the sum of the excitations at different levels  $T = T_1 + T_2 + \dots + T_x$  until  $x$  excitations, then

$$T - T^\dagger = \sum_{a,i}^{n_o-1} \theta_{ai} (c_a^\dagger c_i - c_i^\dagger c_a) + \sum_{a,b,i,j}^{n_o-1} \theta_{abij} (c_a^\dagger c_b^\dagger c_i c_j - c_j^\dagger c_i^\dagger c_b c_a) + \dots \quad (7)$$

where  $a, b \in \text{virt}$ ,  $i, j \in \text{occ}$ ,  $\theta_{ai}$  and  $\theta_{abij}$  are variational parameters associated with their cluster operators. They ensure that UCC applied within VQE can approximate the true ground eigenstate of the system, which is not guaranteed in the case for example of the hardware efficient ansatz, whose parameters are not chemically inspired. Preparing UCC ansatz on a classical computer cannot be easily performed even for low-ordered cluster operators due to the non-truncation of the Baker–Campbell–Hausdorff (BCH) series<sup>61</sup>. On the contrary, it can be prepared on a quantum device, and it has been shown that VQE can yield a final state of right parametrization with a good overlap that preserves the fidelity close to one (e.g. with an overlap  $\langle \psi_{UCC} | \psi_0 \rangle$  close to one, between the converged UCC solution and the FCI solution  $\psi_0$ ).

### 2.2.1 | Implementation of Unitary Coupled Cluster on quantum devices

In this subsection, we describe in detail the implementation of the UCC wavefunction on a quantum computer, which is an important component in the VQE steps described above. The UCC wavefunction in Eq. (6) is implemented on a quantum device by first constructing a circuit corresponding to the qubit representation of the HF state state (by implicitly using JW representation)

$$|\psi_{HF}\rangle_Q = |11110000\dots\rangle$$

where  $|0/1\rangle$  refers to a single qubit being in the state 0 or 1. In the multi-qubit register, we assign each qubit to a spin-orbital, with orbital energies ranging from low to high. The  $|0\rangle$  state refers to an unoccupied spin-orbital, while  $|1\rangle$  refers to an occupied spin-orbital. The device qubit register is initialized to a zero state  $|0000000\dots\rangle$  then by applying a set of (non-parametrized) gate operations (for example, X gates) to  $|0000\dots\rangle$ , the qubit representation of the HF state,  $|\psi_{HF}\rangle_Q$ , is created.

After having  $|\psi_{HF}\rangle_Q$  prepared on the device, the unitary operator  $U(\theta) = e^{T-T^\dagger}$  has to be implemented as well. This is done following these steps:  $U(\theta)$  has to be first decomposed into operations that can be implemented into circuit compatible with present available quantum computers. To do this, in practice,  $U(\theta)$  is approximated using the Trotter decomposition<sup>62,63,64</sup>, which breaks up the exponential of a sum to an ordered product of individual exponentials. Such transformation provides a reasonable approximation to the full unitary operator which is disassembled into local unitary operators. Following Eqs. (1.3-1.6) in<sup>65</sup>, the

formula of trotterized  $U(\theta)$  with  $T - T^\dagger$  (Eq. 7) truncated at  $x = 2$  excitations can be expressed as:

$$U(\theta) \approx \prod_{\rho} \left( e^{\frac{\theta_{\rho}}{t} (T_{\rho} - T_{\rho}^\dagger)} \right)^t + \mathcal{O}(\frac{1}{t}) \quad (8)$$

where  $t$  is the number of Trotter steps and  $\rho$  corresponds to the elements of excitations introduced in Eq. 7. Orders of  $t$  above one can decrease the Trotterization error, however for the current available NISQ devices, it is not recommended since it would involve additional gates induced by the UCC ansatz translation into a quantum-circuit<sup>66,36</sup>. Nevertheless, as is shown in Figure 5 of reference<sup>66</sup>, by using UCCSD method in  $H_2$  molecule, increasing the trotter error does not affect the convergence and the UCCSD energy. In the present work, we use an UCC ansatz truncated at the single and double excitations levels while we employ a single Trotter step. Once these approximations are performed, each exponential of a fermionic excitation operator (see Eq. (8)) can be directly implemented as a quantum circuit, i.e. as a series of parameterized gates  $U(\theta) = U_1(\theta_1)U_2(\theta_2)U_3(\theta_3)\dots U_k(\theta_k)$  applied to the qubits, where  $U_k(\theta_k)$  is the  $k^{\text{th}}$  one- or two-qubit unitary gate, controlled by a  $\theta_k$  parameter. Having  $U(\theta)$  prepared and applied into  $|\psi_{HF}\rangle_Q$ , completes the circuit on the quantum computer that generates  $|\psi_{UCC}\rangle$ .

### 2.2.2 | Exponential mappings

The CNOT staircase<sup>21,25,34</sup> is the standard method to map the exponential of the fermionic excitation evolution (after JW transformation) into a sequence of gates. In theory, the JW transformation relates spin-1/2 operators to fermionic creation and annihilation operators. JW is the basic transformation we used through the article. Mapping the UCC ansatz from this method has been shown to provide accurate results associated to a smooth optimization convergence<sup>21</sup>. However, the cost of using such a method is linked to the increase in the number of CNOT gates, which scales linearly with the system size  $O(n_o)$  when a JW transformation is used<sup>50</sup>. Consequently, it limits the size of molecule that can be tested on available NISQ devices. Nevertheless this method has been extensively tested using different types of fermionic excitation presented in the next section. They include: UCCSD and UCCGSD, k-UpCCGSD ansatze. There are also other types of excitations that generate other versions of the UCC ansatze (see<sup>36</sup> for example) but they are out of the scope of the present work. Additional work has been done towards optimizing the number CNOT counts gates and circuit depth by constructing CNOT- efficient circuits<sup>67,68,69</sup> in order to implement unitary evolutions of single and double qubit excitation operators, which obey to the qubit commutation relations. The resulting circuits require up to 2 (8) times fewer CNOTs in the case of single (double) fermionic excitation evolutions than within the standard method. This type of qubit evolution can be used to construct a new version of the UCC ansatz which is called QUCCSD (see next section). Mappings of both exponentials corresponding to fermionic and qubit excitation evolutions through CNOT staircase and efficient circuit methods are explained in detail in chapter two of<sup>70</sup>, as well as a brief explanation of the definitions of CNOT gates and depth from the two circuit methods.

## 2.3 | Unitary Coupled Cluster approaches truncated at single and double excitations levels

In this subsection we list the different versions of UCC that are truncated at the single and double excitation levels, by defining the excitation generator in each UCC version. We review as well their recent use within variational algorithms. We first focus on the UCCSD and QUCCSD ansatze for comparison purposes on the scale of gate complexity and CNOT counts. We then focus on a second group of methods that includes UCCGSD and k-UpUCCGSD, which as is shown in some reviews, it performs better in term of chemical accuracy than the first group of ansatze. However, it has been shown that such approaches require an increased circuit depth than the first group of techniques. These features have motivated us to implement these versions of UCC together with ADAPT-VQE (presented in the next section) in our Open-VQE package (see sec 4).

### 2.3.1 | UCCSD and QUCCSD ansatze

#### UCCSD:

Unitary Coupled Cluster Single and Double was the first commonly used ansatz by the quantum chemistry community for quantum computing, and it was successfully tested experimentally on quantum computers using VQE<sup>60,34</sup>. Chemically, the UCCSD ansatz includes few excitations of fermionic single and double operators, which occur only from occupied to unoccupied (virtual) spin-orbitals on the top of the HF state. These excitations are given by:

$$\sum_{ai} \theta_{ai} (c_a^\dagger c_i - c_i^\dagger c_a) + \sum_{abij} \theta_{abij} (c_a^\dagger c_b^\dagger c_i c_j - c_j^\dagger c_i^\dagger c_b c_a) \quad (9)$$

where  $a, b \in \text{virt}$ ,  $i, j \in \text{occ}$ . By assuming a single-step Trotter approximation (Eq. (8)), UCCSD is given by the product of single and double fermionic evolutions

$$U(\Theta) = \prod_{a,i} e^{\left(\theta_{ai}(c_a^\dagger c_i - c_i^\dagger c_a)\right)} \prod_{a,b,i,j} e^{\left(\theta_{abij}(c_a^\dagger c_b^\dagger c_i c_j - c_j^\dagger c_i^\dagger c_b c_a)\right)} \quad (10)$$

### QUCCSD:

The Qubit Unitary Coupled Cluster Single and Double method is a simplified version of the UCCSD ansatz (Eq. (10)) in which only single and double excitation are used to construct the trial wavefunction

$$U(\Theta) = \prod_{a,i} e^{\left(\theta_{ai}(q_a^\dagger q_i - q_i^\dagger q_a)\right)} \prod_{a,b,i,j} e^{\left(\theta_{abij}(q_a^\dagger q_b^\dagger q_i q_j - q_j^\dagger q_i^\dagger q_b q_a)\right)}, \quad (11)$$

where  $q_a^\dagger(q_i)$  are the qubit creation (annihilation) operators without the inclusion of Z-Pauli terms after JW transformation (see their expressions in chapter two, section 2.2 (Eqs. 2.11 and 2.12) of<sup>70</sup>). These excitations can be achieved by particle-preserving exchange gate rotations in the qubit space. It differs from UCCSD ansatz, which contains many Z-Pauli terms after JW transformation. The actual role of Z-Pauli is to conserve the parity from fermionic creation (annihilation)  $c^\dagger(c)$  operators, while keeping the time-symmetry and particle conservation. By comparing QUCCSD to UCCSD ansatz VQE performance for a few simple molecules, it has been shown<sup>51</sup> that the two ansätze could achieve a nearly identical accuracy in the estimation of the ground state energies. Even though the parity property is missed in the qubit evolution excitations, it was found, as is explained in previous section, that the advantage of using QUCCSD is to reduce the CNOT counts with respect to the CNOT staircase circuit to implement fermionic evolutions. This demonstrates that QUCCSD is sufficient to approximate the exact FCI wavefunction with a smaller number of gates in the circuit and it might be more favorable for its use on current NISQ devices. However it has been also shown that an unnecessarily large number of parameters and operators occur when the UCCSD and QUCCSD ansatze were used especially when system size gets larger. The increase in parameter and operator counts deepens the circuit which leads to decrease the chemical accuracy in ground state molecular energies. Moreover, these operators may not be ordered in practice and could further decrease the precision. Attempts for keeping ordered operators have been recently proposed.<sup>35,38,41,71</sup>

### 2.3.2 | UCCGSD and k-UpCCGSD ansatze

#### UCCGSD:

Unitary Coupled Cluster Generalized Single and Double has been mentioned first within Nooijen's paper<sup>48</sup>, then latter described in reference<sup>49</sup> for using it in quantum computing applications. It consists in excitations that occur from occupied to occupied, occupied to unoccupied as is expressed in Eq .10, or unoccupied to unoccupied levels:

$$\sum_{pq} \theta_{qp} c_q^\dagger c_p + \sum_{pqrs} \theta_{rspq} c_r^\dagger c_s^\dagger c_q c_p - h.c \quad (12)$$

#### k-UpCCGSD:

Unitary Pair Couple Cluster with Generalized Single and Double Product<sup>49</sup>, where k denotes the products of unitary paired generalized double excitations, along with the full set of generalized single excitations. In other words, single excitation operators are fully generalized without any specific constraint on the choice of occupied and virtual orbitals, but the double excitation operators are generalized and restricted to transitions of pair electrons acting on the same orbital.

$$T_2 - T_2^\dagger = \sum_{q_\alpha q_\beta p_\alpha p_\beta} \theta_{q_\alpha q_\beta p_\alpha p_\beta} c_{q_\alpha}^\dagger c_{q_\beta}^\dagger c_{p_\beta} c_{p_\alpha} - h.c \quad (13)$$

It was recently demonstrated<sup>49,72</sup>,that the UCCGSD ansatz leads to more accurate results for ground state energies than the simpler UCCSD . In the same work, it was shown that starting from k=3 (i.e 3-UpCCGSD) brings better accuracy than UCCSD ansatz (see for example table 4 for H<sub>4</sub> molecule using 6-31G basis set). Indeed, such approaches were also engineered not only for ground states but also to tackle excited states without undesired spin symmetry crossing over to lower states during VQE optimizations. They have been also used in connection with the variational Quantum Deflation algorithm (VQD), that is used to determine the energies of the ground and excited states<sup>73</sup>.

## 2.4 | Adaptive Derivative-Assembled Pseudo-Trotter-VQE (ADAPT-VQE)

Instead of a fixed-length ansatze, other types of iterative variational algorithms have been proposed by the community<sup>74,75,76,77,78</sup>. There are two reasons for that: (1) the fixed-length ansatze use unnecessarily excitations that can be considered as redundant terms as they do not contribute to approximate the FCI wavefunction. This creates longer circuit depth and consumes a greater number of variational parameters. (2) fixed-length ansatze such as UCCSD or QUCCSD cannot provide a good chemical accuracy for strongly correlated systems<sup>51</sup> (i.e. see for example the H<sub>6</sub> molecule in section 5). This problem occurs at long bond length and could be solved by including higher-order excitations and/or using multiple-step Trotterization in the UCCSD or QUCCSD ansatz. Yet, both of these suggestions are problematic since they would necessarily deepen the circuits and increase the number of variational parameters. Fixed-length ansatze like 3-UpCCGSD (or k>3) and UCCGSD might also provide very good accuracy at these bond lengths, because excitations considered are general. However, this yields many redundant terms during optimization, and as the system size increases, the number of operators and parameters increase as well as the circuit depth. Therefore, the ADAPT-VQE approach was an important step toward treating these issues<sup>41,50</sup>. The ADAPT-VQE algorithm constructs the molecular system's wavefunction dynamically and mainly can throughput all these redundant terms. It is grown iteratively in a form of disentangled UCC ansatz as given in Eq. (14). Operators are defined in a pool, in which the operator (few operators) contributing to the largest energy deviations is(are) chosen and added gradually to the ansatz until the exact FCI wavefunction has been reached (see below in subsubsection 2.4.1 steps of the algorithm). This process allows reaching this goal faster than with the UCC-family ansatze. For example, within the normal UCCSD-VQE, we would need several trotterization steps to reach a certain chemical accuracy to find the exact FCI. Conversely, with the ADAPT-VQE algorithm and to obtain the same level of accuracy, the ansatz requests fewer variational parameters, and a correspondingly shallower circuit containing a smaller number of gates. The FCI wave function approximated within arbitrary accuracy from ADAPT-VQE is given by

$$\prod_{k=1}^{\infty} \prod_{pq} \left( e^{\theta_{pq}(k) \hat{A}_{pq}} \prod_{rs} e^{\theta_{pqrs}(k) \hat{A}_{pq,rs}} \right) |\psi_{HF}\rangle, \quad (14)$$

which is in the form of a long product of one- $\hat{A}_{pq}$  and two-body  $\hat{A}_{pq,rs}$  general operators generated from the pool of excitations,

where each of the variational parameters  $\{\theta_{pq}, \theta_{pqrs}\}$  is associated to an operator. Historically, fermionic ADAPT-VQE<sup>41</sup> was the first algorithm in the family of adaptive ansatze. The name "fermionic" comes from the excitation pool operators formed as spin-complement pairs of single and double fermionic evolutions (see Eqs. A1 and A2). The fermionic ADAPT-VQE has been shown to bring accurate chemical results for several molecules such as for H<sub>4</sub>, LiH and H<sub>6</sub> molecules (as shown in figure 2 of<sup>41</sup> by using an ansatz constituted of fewer parameters and shorter circuit depth than for the corresponding UCCSD results).

Further work has been focused on proposing qubit ADAPT-VQE<sup>50,52</sup>, as the motivation was toward reducing the circuit gates more efficiently than with fermionic ADAPT-VQE. In the fermionic case, each fermionic operator transfers into eight-Pauli strings (after JW transformation) including their Hermitian conjugates. When we want to map the exponential for each of these Pauli-strings into circuits, using the CNOT staircase method, the Pauli strings correspond to "single" fermionic excitations will request 4 CNOT staircase and those of double" fermionic excitations will request 16 CNOT staircase. In qubit ADAPT-VQE, the pool used is a collection of anti-Hermitian operators where each operator consists of a string that contains a tensor product of Pauli matrices. In qubit ADAPT-VQE each string is transpiled into a defined number of CNOT gates using the CNOT staircase method, but unlike the fermionic ADAPT-VQE, the qubit ADAPT-VQE produces a smaller number of gates at the end of the process. Qubit ADAPT-VQE has been tested for several molecules<sup>50</sup>, showing that the circuit is shallower- the number of gates being reduced by one order of magnitude compared to fermionic ADAPT-VQE. However qubit ADAPT-VQE requests a higher number of parameters and iterations in order to reach a certain level of chemical accuracy.

The cost of fermionic- and qubit-ADAPT-VQE is the number of measurements which scales  $O(n^8)$ <sup>41,50</sup> needed to compute the energy gradients, where  $n$  represents the number of qubits. The choice of pool in qubit ADAPT-VQE has also been important in the research to reach and approximate the FCI wavefunction, with a view to not only reduce the circuit depth compared to fermionic ADAPT-VQE but also to minimize the number of operators in the pool without losing the completeness properties of operators. Reducing the pool size from  $O(n^4)$  into  $2n - 2$  operators and maintaining the necessary and sufficient conditions for completeness has been achieved in a recent work<sup>52</sup>. This new scale of pool size reduces the number of measurements from  $O(n^8)$  to  $O(n^5)$  for a given molecular system. In the same reference, it was shown that incorporating symmetries into the pool solves the convergence problems caused by the lack of symmetries.

### 2.4.1 | Implementing fermionic or qubit ADAPT-VQE algorithms

Here we describe the procedure to implement the fermionic or qubit-ADAPT-VQE. The first three steps present the essential components for implementing the algorithm and the rest of steps describes the iterative loop in ADAPT-VQE:

1) In the ADAPT-VQE, the computation of one-body and two-body integrals is performed with a chemistry package such as pySCF. This allows one to write the Hamiltonian in the second-quantization form given by Eq. 2. This Hamiltonian is transformed into a qubit representation by using a spin transformation (see section 2.1 Eq. 4).

2) One has to define the pool of operators of size  $m$ . We can have two types of pools, the first is of fermionic nature and the second is related to qubit, depending on the ADAPT-VQE variant used. Within a fermionic ADAPT approach, the pool is defined as  $F_m = \{F_m(p, q), F_m(p, q, r, s)\}$  and consists of one-  $F_m(p, q)$  and two-  $F_m(p, q, r, s)$ - body unitary generalised fermionic excitations.  $F_m$  are considered as the set of all unique spin-complemented one- and two-body operators, as they are given in eqs. A1 and A2. In the qubit ADAPT case, the pool is defined as single and double qubit evolutions,  $Q_m = \{Q_m(p, q), Q_m(p, q, r, s)\}$  (for more details about the nature of these operators, one can refer to subsubsection 5.3.3).

3) A reference Hartree-Fock  $|\psi_{HF}\rangle$  state needs to be chosen in the qubit representation that preserves the number of electrons of the system. At this stage, it is then possible to construct the ansatz by starting the ADAPT-VQE-iteration at  $k = 1$ . The ansatz is initialized by the identity  $U^{(0)}(\theta) = I$  and then it is actually represented by the HF state. Then the loop starts (by a "while loop" until exit) of the ADAPTIVE wavefunction as follows.

4) Then the trial state with the current ansatz on the quantum simulator  $|\psi^{(k-1)}\rangle = U^{k-1}(\theta_{k-1})|\psi_{HF}\rangle$ , where  $\theta_{k-1}$  comes from the previous VQE-iteration, has to be prepared.

5) In order to obtain the energy gradient, the commutator has to be measured between the Hamiltonian  $H$  and each of the operators in the pool. For the fermionic ADAPT-VQE case, the exponential for each of unitary fermionic operator in  $F_m$  and the gradient is the derivative of energy over  $\theta_{k-1}$ :

$$\frac{\partial E^{(k-1)}}{\partial \theta_m} = \langle \psi(\theta_{k-1}) | [H, F_m] | \psi(\theta_{k-1}) \rangle. \quad (15)$$

For the Qubit-ADAPT-VQE case, the exponential for each of unitary fermionic operator in  $Q_m$ , and the gradient is the derivative of energy over  $\theta_{k-1}$ :

$$\frac{\partial E^{(k-1)}}{\partial \theta_m} = \langle \psi(\theta_{k-1}) | [H, Q_m] | \psi(\theta_{k-1}) \rangle \quad (16)$$

6) If the norm of the gradient vector

$$\|g^{(k-1)}\| = \sqrt{\left(\frac{\partial E^{(k-1)}}{\partial \theta_1}\right)^2 + \dots + \left(\frac{\partial E^{(k-1)}}{\partial \theta_m}\right)^2} \quad (17)$$

becomes smaller than a threshold,  $\epsilon$ , then there is an exit of the loop.

7) The operator with the largest gradient is then found

$$\max_{\theta_i} \left( \left| \frac{\partial E^{(1)}}{\partial \theta_1} \right|, \left| \frac{\partial E^{(2)}}{\partial \theta_2} \right|, \dots, \left| \frac{\partial E^{(k-1)}}{\partial \theta_m} \right| \right)$$

and this single operator is added to the left end of the ansatz, with a new variational parameter  $\theta_k = \theta_i$ . The wavefunction corresponding to fermionic and qubit ADAPT are given respectively by:

$$|\psi^{(k)}\rangle = e^{\theta_k F_k} |\psi^{(k-1)}\rangle = e^{\theta_k F_k} \dots e^{\theta_3 F_3} e^{\theta_2 F_2} e^{\theta_1 F_1} |\psi_{HF}\rangle \quad (18)$$

$$|\psi^{(k)}\rangle = e^{\theta_k Q_k} |\psi^{(k-1)}\rangle = e^{\theta_k Q_k} \dots e^{\theta_3 Q_3} e^{\theta_2 Q_2} e^{\theta_1 Q_1} |\psi_{HF}\rangle \quad (19)$$

8) Perform a VQE experiment to re-optimize all parameters  $\{\theta_k, \theta_{k-1}, \dots, \theta_2, \theta_1\}$  in the ansatz.

9) When this is over we go back to step 4.

Detailed information about the procedure of making fermionic- and qubit-ADAPT-VQE can be also found in section "Results" of<sup>41</sup>.

### 3 | ALGORITHMS FOR QUANTUM CHEMISTRY ON THE ATOS QUANTUM LEARNING MACHINE

In this section, we briefly review the tools of the Atos Quantum Learning Machine (QLM) that are relevant for quantum chemistry computations. We will then, in the next section (sec. 4), describe how we build an advanced chemistry module upon these tools.

#### 3.1 | A quantum programming environment and a powerful simulator

QLM is a complete environment designed for quantum software programmers, engineers and researchers<sup>79</sup>. It includes a wide variety of low-level tools useful for writing, compiling and optimizing quantum circuits<sup>80,81,82,83,84</sup>. These tools come in the form of so-called "plugins" that can be combined or stacked upon another to construct a quantum compilation chain.

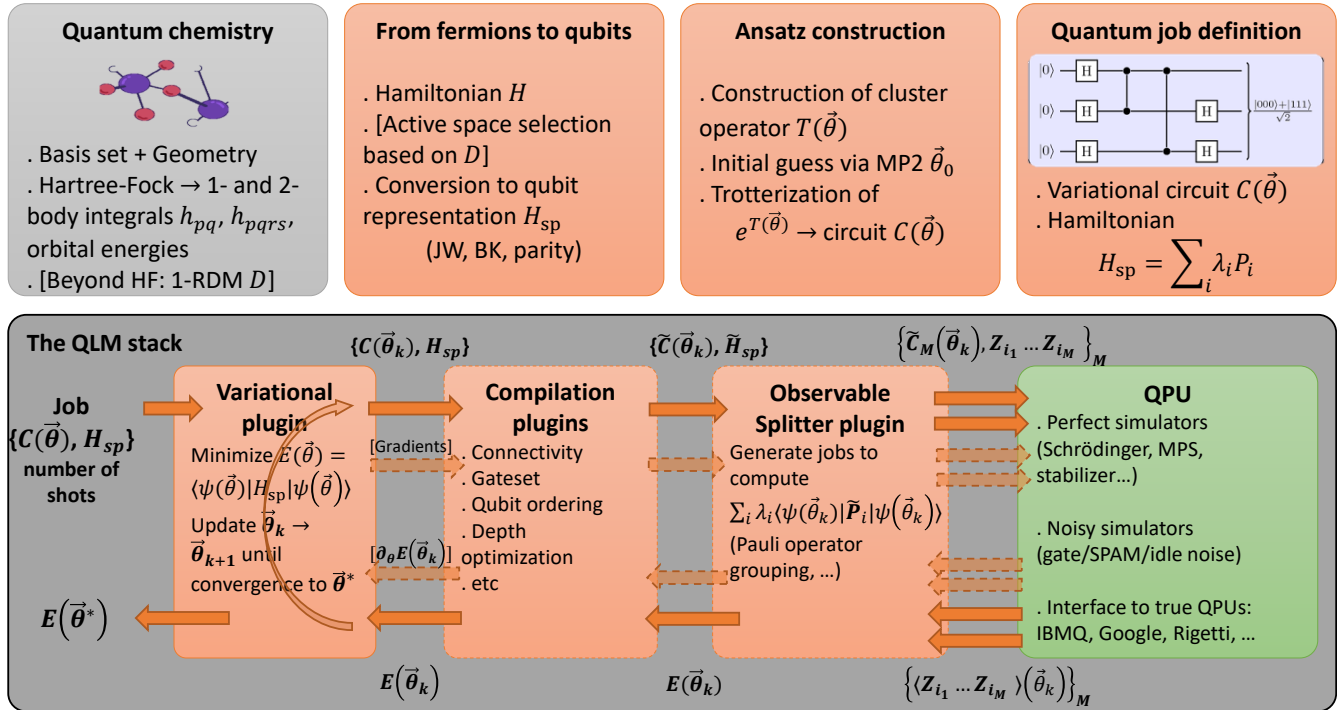


**FIGURE 1** QLM workflow for quantum chemistry. *Top row:* Steps to prepare a variational quantum job containing a parameterized circuit and the Hamiltonian whose ground state energy one wants to approximate. The leftmost (grey) box uses standard third-party quantum chemistry modules. Orange boxes stand for QLM libraries. *Bottom row:* QLM stack, with plugins (orange boxes) that pre- and post-process the job and results, and a QPU (green box) that executes the quantum job and returns a result.

QLM can simulate quantum circuits in a noiseless or noisy fashion. The noiseless simulators come in different flavors, with "Schrödinger style" simulators (storing the wavefunction either in a dense fashion or using Matrix Product States<sup>85</sup>), a "Feynman-style" simulator<sup>86</sup>, a binary decision diagram simulator<sup>87</sup>, a Clifford simulator, etc. The Schrödinger-style dense simulator can reach up to 41 qubits for any circuit, while the other simulators can reach much larger qubit counts depending on the circuit properties (entanglement, gateset, etc). The noisy simulators enable the emulation of realistic quantum noise, a crucial tool in the current NISQ era. Gate noise, State Preparation and Measurement (SPAM) noise and idling noise can be taken into account via density-matrix (resp. stochastic) simulations that can handle circuit with up to 20 (resp. 40) qubits. Most importantly, the interface of the simulators (also called "Quantum Processing Units" or QPUs) is such that they can easily be swapped for actual experimental QPUs without modifying the quantum program. QLM provides an interface to various hardware processors including those constructed by IBM and Rigetti. Its circuits are also interoperable<sup>44</sup> with other quantum circuit descriptions like Qiskit<sup>45</sup>, Cirq<sup>46</sup> and PyQuil<sup>47</sup>, as described in more detail in Appendix B. Moreover, QLM comes with quantum application

libraries that enable the easy exploration of potential use cases of quantum computing. These libraries help generate quantum programs in fields ranging from combinatorial optimization to quantum chemistry and condensed-matter physics.

A summary of the QLM workflow for quantum chemistry is provided in figure 1 . The top row represents the steps one has to go through to handle a quantum chemistry problem using `myQLM-fermion` (bracketed terms represent optional steps). At the end of these steps, one obtains a "job" comprising a parameterized quantum circuit (that implements a UCC ansatz)  $C(\vec{\theta})$  and a Hamiltonian  $H_{\text{sp}}$  represented as a sum of Pauli terms. This job can then be fed to the QLM stack. This stack, represented in the bottom row, can be constructed by the user at will depending on the QPU they want to execute the job on. A minimal stack consists of a QPU (without plugins), which can handle minimal jobs containing native quantum circuits (with gates native to the hardware and compliant with its connectivity) and  $Z$ -axis observables. To handle more sophisticated jobs, one can stack "plugins" on top of the QPU. Each plugin has a well-defined role, such as compiling the circuit to a given gateset, rewriting it to comply with a given connectivity (see "Compilation plugins"), or generating all the elementary jobs required to compute the expectation value of a general observable (see "Observable Splitter plugin"). Finally, some plugins can handle variational jobs corresponding to the VQE algorithm. Such "variational plugins" handle the update of the variational parameters based on the result of the previous steps. They can optionally generate jobs to compute the gradient of a given expectation value if gradient-based optimization is asked for.

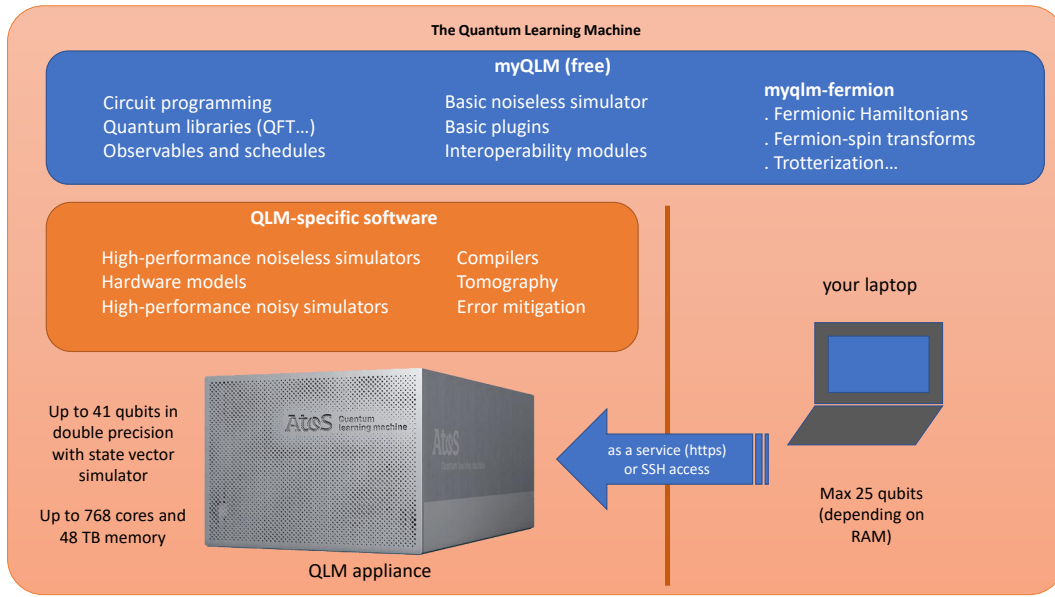


**FIGURE 2** Overview of the QLM environment. Documentation of my-QLM/myQLM-fermion is given in<sup>43,54</sup>.

In practice, the QLM environment is composed of software modules and a powerful classical HPC hardware appliance, as described in figure 2 . Among the software modules, some are available and downloadable for free as Python packages. They come under the name of `myQLM`<sup>43</sup>. `myQLM` includes modules for programming quantum circuits, with quantum libraries (for performing e.g quantum arithmetic operations, etc), for describing quantum observables and analog quantum schedules. It also comes with a basic noiseless simulator for quantum circuits, basic plugins (e.g for splitting observables depending on the commutation relations of the Pauli operators), and modules for interacting with other quantum frameworks like Qiskit, Cirq, etc. Finally, `myQLM` contains the aforementioned `myQLM-fermion` module. `myQLM` can be installed on a laptop or on a local cluster. The size of the circuits that can be simulated with the QPU simulator of `myQLM` is limited by the available Random Access Memory (RAM) (for a standard laptop, this corresponds to about 25 qubits). The Quantum Learning Machine is also a powerful HPC appliance. It comes with extra software in addition to `myQLM`: advanced noiseless simulators, modules for describing hardware models, noisy simulators (both gate-based and analog), advanced compilers, tomography and error mitigation modules, among others. The appliance itself can simulate circuits with up to 41 qubits when using state vector simulators, and more when using more specific representations of the wave function (like Matrix Product States or stabilizers). The software module we present below, Open-VQE, relies only on `myQLM` modules, which means it can be used by simply downloading `myQLM` on one's

personal machine. Therefore, the results shown for small qubit counts can be (up to the run times) reproduced on a personal laptop. In practice, to execute the simulations, we used the QLM advanced noiseless statevector simulator so as to reach large qubit counts and gain speed.

### 3.2 | myQLM-fermion: An Open Source QLM module for fermionic many-body problems

The tools for quantum chemistry are collected into an open-source module called "myQLM-fermion", which is part of myQLM. myQLM-fermion provides general tools for dealing with fermionic problems: representations of fermionic Hamiltonians (including usual Hamiltonians like the electronic structure Hamiltonian (Eq. (2)), the Hubbard and Anderson Hamiltonians), transformations from fermion operators to qubit operators (Jordan-Wigner, Bravyi-Kitaev, parity), generation of quantum evolution circuits via Trotterization, implementation of the quantum phase estimation algorithm, as well as various modules for variational algorithms such as VQE (see subsection 2.1): libraries of variational ansätze (like hardware-efficient ansätze, matchgate circuits, Low-Depth Circuit ansatz (LDCA) circuits), various optimization plugins (including the standard optimizers implemented in `scipy`<sup>57</sup> (COBYLA, BFGS, etc) as well as the Simultaneous Perturbation Stochastic Algorithm (SPSA) and Particle-Swarm Optimizer (PSO)).

A submodule of myQLM-fermion<sup>54</sup> is specifically devoted to quantum chemistry. It provides tools for selecting active spaces (based on natural-orbital occupation numbers), generating cluster operators (and thus, via the aforementioned Trotterization tools, UCC-type ansätze), and initial guesses for their variational parameters. The architecture of QLM and myQLM-fermion allows for experts in a given field to construct their own advanced modules with the QLM building blocks.

The key building block of quantum chemistry computations is the Hamiltonian, Eq. 2. On QLM, it is described by an object `ElectronicStructureHamiltonian`

```
1 from qat.fermion import ElectronicStructureHamiltonian
2 hamiltonian = ElectronicStructureHamiltonian(h, g)
```

where `h` and `g` are the tensors  $h_{pq}$  and  $h_{pqrs}$  of Eq. (2). Such an object also describes cluster operators such as the ones described in Eq. (9). For instance, the following snippet

```
1 from qat.fermion import get_cluster_ops
2 cluster_ops = get_cluster_ops(n_electrons, nqubits=nqubits)
```

creates the list containing the sets of single excitations  $\{c_k^\dagger c_i - c_i^\dagger c_k, k \in \text{virt}, i \in \text{occ}\}$  and double excitations  $\{c_l^\dagger c_k^\dagger c_j c_i - c_j^\dagger c_i^\dagger c_l c_k, k, l \in \text{virt}, i, j \in \text{occ}\}$ .

These objects can be readily converted to a spin (or qubit) representation using various fermion-spin transforms:

```
1 # Jordan-Wigner
2 from qat.fermion.transforms import transform_to_jw_basis
3 hamiltonian_jw = transform_to_jw_basis(hamiltonian)
4 cluster_ops_jw = [transform_to_jw_basis(t_o) for t_o in cluster_ops]
5
6 # Bravyi-Kitaev
7 from qat.fermion.transforms import transform_to_bk_basis
8 hamiltonian_bk = transform_to_bk_basis(hamiltonian)
9 cluster_ops_bk = [transform_to_bk_basis(t_o) for t_o in cluster_ops]
```

The transformed objects are now in the form of Eq. (4). With these qubit operators, one can then easily construct a simple UCCSD ansatz via trotterization of the exponential of the parametric cluster operator defined in Eq. (9):

```
1 from qat.lang.AQASM import Program, X
2 from qat.fermion.trotterisation import make_trotterisation_routine
3
4 prog = Program()
5 reg = prog.qalloc(nqubits)
6 # Create Hartree-Fock state (assuming JW representation)
7 for qb in range(n_electrons):
8     prog.apply(X, reg[qb])
9
10 # Define the full cluster operator with its parameters
11 theta_list = [prog.new_var(float, "\\\theta_{%s}" % i) for i in range(len(cluster_ops_jw))]
12 cluster_op = sum([theta * T for theta, T in zip(theta_list, cluster_ops_jw)])
13
14 # Trotterize the Hamiltonian (with 1 trotter step)
15 qrout = make_trotterisation_routine(cluster_op, n_trotter_steps=1, final_time=1)
16 prog.apply(qrout, reg)
17 circ = prog.to_circ()
```

The circuit we constructed, `circ`, is a variational circuit that creates a variational wavefunction  $|\psi(\theta)\rangle$ . Its parameters can be optimized to minimize the variational energy, Eq. (5). This is done by a simple VQE loop:

```

1 # create a quantum job containing the variational circuit and the Hamiltonian
2 job = circ.to_job(observable=hamiltonian_jw, nbshots=0)
3
4 # import a plugin to perform the optimization
5 from qat.plugins import scipyMinimizePlugin
6 optimizer_scipy = scipyMinimizePlugin(method="COBYLA", tol=1e-3, options={"maxiter": 1000}, x0=theta_init)
7
8 # import a QPU to execute the quantum circuit
9 from qat.qpus import get_default_qpu
10
11 # define the quantum stack
12 stack = optimizer_scipy | get_default_qpu()
13
14 # submit the job and read the result
15 result = stack.submit(job)
16
17 print("Minimum energy =", result.value)

```

The simulated QPU used in the previous code snippet can be readily replaced by an actual QPU by using the `qat-interop` module. For instance, in the following snippet, we use a transmon QPU by IBM:

```

1 from qat.interop.qiskit import BackendToQPU
2 qpu= get_default_qpu()
3 qpu = BackendToQPU(token=MY_IBM_TOKEN, ibmq_backend="ibmq_guadalupe")

```

Conversely, circuits created using other quantum programming frameworks can be converted to the QLM format. For instance, here we convert a circuit written in the Google Cirq format to a QLM circuit (that can then be fed to a QLM simulator):

```

1 from qat.interop.cirq import cirq_to_qlm
2 qlm_circ = cirq_to_qlm(your_google_circ)

```

## 4 | THE OPEN-VQE PACKAGE

The implementation of Open-VQE facilitates the development of new algorithms on quantum computers. It consists in a couple of new modules that extend the main myQLM/myQLM-fermion implementations (see section 3 above). Those modules allow to build normal UCCSD algorithm, its variants and ADAPT-VQE's algorithms as reviewed in section 2. To explain in another fashion, Open-VQE allows to perform calculations using new types of UCC methods that are different from the QLM predefined ones such as the regular UCCSD ansatz.

Open-VQE consists of two main modules which are inside "openvqe" folder given as follows:

- **UCC Family** denoted in code by "ucc\_family": this module includes different classes and functions to generate the fermionic cluster operators (fermionic pool) and the qubit pools, and to get the VQE optimized energies in the cases of active and non-active orbital selections.
- **ADAPT** denoted by "adapt": it includes two sub-modules which are:
  - **Fermionic-ADAPT**: containing functions performing the fermionic ADAPT-VQE algorithmic steps in the active and non-active space selections.
  - **Qubit-ADAPT**: containing functions that perform the qubit ADAPT-VQE algorithmic steps calculation in the active and non-active space orbital selections.

Additionally "openvqe" contains a subfolder named "common\_files" that stores all the internal functions needed to be imported for executing the two modules. Open-VQE consists also a "notebooks" folder that allows the user to run and test the above two modules which are theoretically described in the review section 2. In our GitHub website<sup>53</sup> we describe the package and the codes allowing for performing these modules. The brief sketch of Open-VQE implementation is explained in the flow chart presented in figure 3 . We remind the reader that we will describe below the code of Open-VQE that studies the full space selections and the codes which are related to active space selections can be found in the GitHub website<sup>53</sup> inside "notebooks"

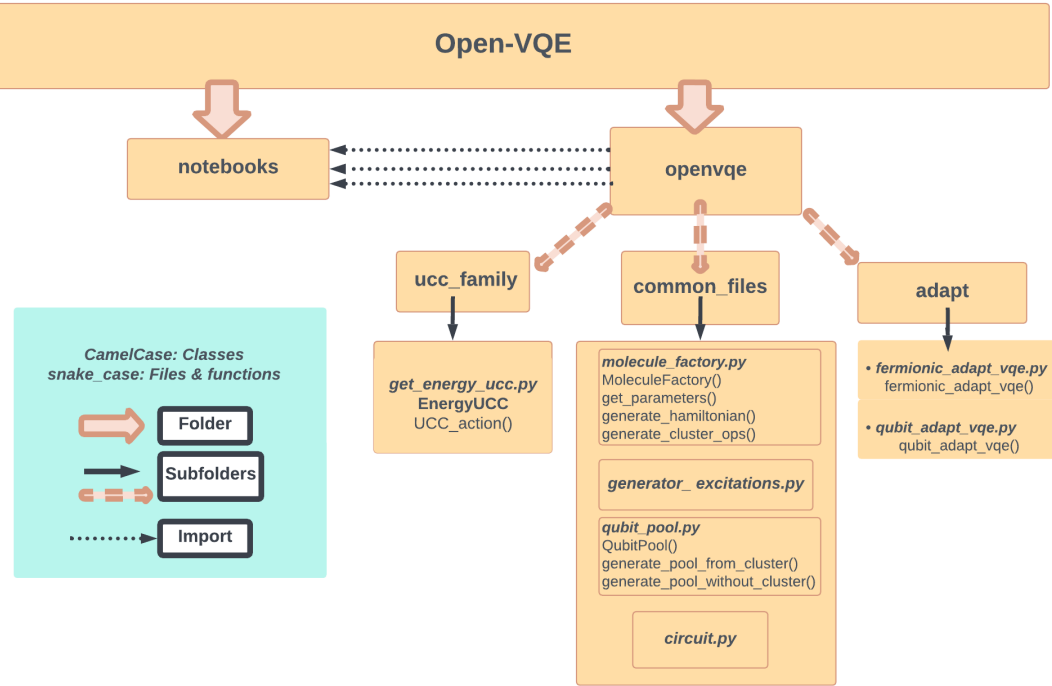


**FIGURE 3** Flow chart of the Open-VQE package. The code is given in our Github repository and documentation<sup>53</sup>.

with prefix "active\_space" and the tools provided in documentation of<sup>54</sup>. In order to develop a new algorithm using our Open-VQE package, it is important to list the different parameters and return variables contained in its main functions. In what follows we describe the snippets python codes which are written in the "tutorials" folder. Then, we describe the snippet codes related to some internal functions related to "ucc\_family" and "adapt", respectively.

The first crucial parameters are the ones specifying the characteristics of the molecules such as symbol of the molecule; the type of excitation generator, which are generators to produce the excitations that found in sec. 2.3: UCCSD (Eq. 9), QUCCSD (Eq. 11), UCCGSD (Eq. 12), K-UpCCGSD (Eq. 13) and spin-complemented pair (Eq. A1 and Eq. A2); the spin transformation mapping (JW, Bravyi-Kitaev, parity basis), choice of active or non-active space selection, denoted respectively in our code as molecule\_symbol, type\_of\_generator, transform, and active.

```

1 # molecule examples: H2, H4, H6, LiH, H2O, CO, CO2, NH3 etc...
2 molecule_symbol = 'H2O'
3 # suppose user choose the spin-complemented generalized singlet and doublet denoted as spin_complement_gsd
4 type_of_generator = 'spin_complement_gsd'
5 # user can type other type of generators, such as: uccsd, quccsd, uccgsd, k-upccgsd, etc...
6 # we type Jordan wigner (JW), user can also type Bravyi-Kitaev or Parity basis
7 transform = 'JW'
8 # no active space selection, set:
9 active = False
10 # for active space (AS), switch to "active = True"

```

The user specifies these parameters in a class called MoleculeFactory. This class takes those parameters as input:

```

1 from openvqe.common_files.molecule_factory import MoleculeFactory
2 # returns the properties of a molecule:
3 r, geometry, charge, spin, basis = MoleculeFactory.get_parameters(molecule_symbol = 'H2O')

```

define a function named as generate\_hamiltonian that generates the electronic structure Hamiltonian (hamiltonian) and other properties such as the spin hamiltonian (for example hamiltonian\_jw), number of electrons (n\_electrons), the list contains the number of natural orbital occupation numbers (noons\_full), the list of orbital energies (orb\_energies\_full)<sup>1</sup> and info<sup>2</sup>:

<sup>1</sup>orbital energies are doubled due to spin degeneracy

<sup>2</sup>a dictionary that stores energies of some classical methods: Hartree-Fock, CCSD and FCI

```

1 # use myQLM-fermion tools to construct generate_hamiltonian():
2 from qat.fermion import ElectronicStructureHamiltonian
3 from qat.fermion.chemistry.pyscf_tools import perform_pyscf_computation
4 from qat.fermion.chemistry.ucc import (convert_to_h_integrals, transform_integrals_to_new_basis)
5 from qat.fermion.transforms import (get_jw_code, recode_integer, transform_to_jw_basis)
6
7 Hamiltonian, hamiltonian_jw, n_els, noons_full, orb_energies_full, info = MoleculeFactory.generate_hamiltonian(
8     molecule_symbol='H2O', active=False, transform='JW')

```

In addition to that, we define another function named as `generate_cluster_ops()` that takes as input the name of excitation generator user need (e.g., UCCSD, QUCCD, UCCGSD, etc.) and internally it calls the file name `generator_excitations.py` which allows `generate_cluster_ops()` to return as output the size of pool excitations, fermionic operators, and JW transformed operators denoted in our code respectively as `pool_size`, `cluster_ops` and `cluster_ops_jw`:

```

1 # for normal uccsd case we use myQLM-fermion tool function:
2 from qat.fermion.chemistry.ucc_deprecated import get_cluster_ops_and_init_guess
3 # we put get_cluster_ops_and_init_guess in the generator_excitations.py together with the other types:
4 from .generator_excitations import (uccsd, quccsd, singlet_gsd, singlet_sd, singlet_upccgsd, spin_complement_gsd,
5     spin_complement_gsd_twin)
6 pool_size, cluster_ops, cluster_ops_jw = MoleculeFactory.generate_cluster_ops(molecule_symbol='H2O',
7     type_of_generator='spin_complement_gsd', transform='JW', active=False)
8 # in our example 'spin_complement_gsd':
9 def generate_cluster_ops():
10     pool_size, cluster_ops, cluster_ops_jw = None, None, None
11     if type_of_generator == 'spin_complement_gsd':
12         pool_size, cluster_ops, cluster_ops_jw = spin_complement_gsd(n_el, n_orb, 'JW')
13     # elif for other excitations (uccsd, quccsd, singlet_upccgsd...)
14     # :::
15     return pool_size, cluster_ops, cluster_ops_jw

```

Once these are generated, we import them as input to the UCC-family and ADAPT modules.

In the UCC module, we have two types of pools: fermionic pool and qubit pool. For the fermionic case, it is determined by the `generate_cluster_ops()` function which is defined before. For the qubit pool, we defined a `QubitPool` class that determines the qubit cluster operators we name as `returned_pool`. Due to the variety of choices of qubit pools, we created two functions in the `QubitPool` class. These functions are in the code defined as follows: `generate_pool_from_cluster()` and `generate_pool_without_cluster()`. The first function takes as parameters the pool name and return the pool with its size. The pools that are accessible for the user are as follows: *full*, *full\_without\_Z* and *reduced\_without\_Z*. However the function `generate_pool_without_cluster()` takes as parameters the type of pool, pool generated from cluster operators and returns the pool with its size. The type of pool that are considered as options for the user are as follows (subsubsection 5.3.3 describes the nature of these pools): *YXXX*, *XYXX*, *XXYX*, *XXXY*, *random*, *two*, *four*, *symmetry*.

```

1 from openvqe.common_files.qubit_pool import QubitPool
2 # number of qubits:
3 nbqubits = hamiltonian_jw.nbqubits
4 # suppose user selects the pool_condition='full_without_Z' then:
5 pool_size, returned_pool = QubitPool.generate_pool_from_cluster(pool_condition, cluster_ops, nbqubits)
6 # Pools are related to qubit cluster operators suppose user selects pool_type = 'two' then:
7 pool_type = 'two'
8 # for some pools such as pool_type = 'symmetry', we need to import the molecule_symbol in the function
9 pool_size, returned_pool = QubitPool.generate_pool_without_cluster(pool_type=pool_type, nbqubits=nbqubits,
10     qubit_pool=cluster_ops_jw, molecule_symbol='H2O')

```

We also provide other functions that can be used by the user (e.g., `qubit_excitations()`) which could be used for performing other type of VQE algorithms such as for QEB-VQE developed by Yordan et al.<sup>69</sup>). Once the fermionic or qubit pool is generated, we call the `get_energies()` from the `EnergyUCC` class in order to obtain the minimal energy calculated with the basic VQE algorithm.

```

1 from openvqe.ucc_family.get_energy_ucc import EnergyUCC
2 # initial guesses theta_1(2) can be MP2 guess, random intervals or fixed values
3 # 1. from UCC-family (with returned pool = ansatz_ops and theta-1)
4 # 2. from UCC-family but with qubit evolutions i.e from "Qubit Pool" (with returned pool = ansatz_q_ops and
5     theta-2)
iterations, result = EnergyUCC.get_energies(hamiltonian_jw, ansatz_ops, ansatz_q_ops, hf_init_sp, theta_1, theta_2, fci)

```

The `EnergyUCC` class performs the required steps to construct the VQE algorithm (see section 2.1) and allows to prepare the UCC ansatz using standard or efficient circuits. These functions call the user-specified classical optimization algorithm (such as BFGS, COBYLA), and returns `iterations`, `results` as dictionaries that would contain: (i) the number of classical parameters used,

(ii) the number of CNOT gates used in the circuit<sup>3</sup>., (iii) the total number of Pauli-string evaluations, (iv) optimized energy ( $E_0$ ) and (v) energy subtracted from the full configuration interaction (FCI). As it is mentioned in previous section, plugins can be used to perform optimization. We can also have another option for optimization use the classical library `scipy.optimize`:

```

1 from qat.lang.AQASM import Program
2 from qat.qpus import get_default_qpu
3 import scipy.optimize
4 # Example
5 theta_optimized_1 = []
6 # define tolerance: the precision goal for the value of energy in the stopping criterion.
7 tolerance=10**(-5)
8 method = "BFGS"
9 opt_result1 = scipy.optimize.minimize(lambda theta: self.ucc_action(theta_1,hamiltonian_jw,ansatz_ops, hf_init_sp
    ),x0=theta_1, method=method, tol=tolerance, options={'maxiter': 50000, 'disp': True})
10 # optimized parameters
11 xlist1 = opt_result1.x
12 # explicit form of UCC_action function is to build the ucc ansatz and execute the circuit on QPU:
13 # from myQLM-fermion we need:
14 from qat.fermion.chemistry.ucc_deprecated import build_ucc_ansatz
15 # build_ucc_ansatz function internally uses the make_spin_hamiltonian_trotter_slice function to build the HF
    state in integer representation and to implement the UCC ansatz applied to HF state.
16 def ucc_action(self,theta_1,hamiltonian_jw,ansatz_ops, hf_init_sp):
17     qpu = get_default_qpu()
18     prog = Program()
19     reg = prog.qalloc(hamiltonian_jw.nbqubits)
20     for n_term, (term, theta_term) in enumerate(zip(ansatz_ops, theta_1)):
21         init = hf_init_sp if n_term == 0 else 0
22         # n_steps is the trotter step
23         qprog = build_ucc_ansatz([term], init, n_steps=1)
24         prog.apply(qprog([theta_term]), reg)
25         circ = prog.to_circ()
26         job = circ.to_job(job_type='OBS', observable=hamiltonian_jw)
27         res = qpu.submit(job)
28     return res.value

```

In the fermionic ADAPT sub-module, we call the function `fermionic_adapt_vqe()` that takes as parameters the fermionic cluster operators, spin Hamiltonian, maximum number of gradients to be taken per iteration, the type of optimizer, tolerance, threshold of norm ( $\epsilon$ ) and the maximum number of adaptive iterations:

```

1 from openvqe.adapt.fermionic_adapt_vqe import fermionic_adapt_vqe
2 # choose maximum number of gradients (1,2,3...)
3 n_max_grads = 1
4 # choose optimizer needed (COBYLA, BFGS, SLSQP, Nelder-Mead etc...)
5 optimizer = 'COBYLA'
6 tolerance = 10**(-6)
7 # according to a given norm value we stop the ADAPT-VQE loop
8 type_conver = 'norm'
9 threshold_needed = 1e-2
10 # the maximum external number of iterations to complete the ADAPT-VQE under a given threshold_needed
11 max_iterations = 35
12 fci = info['FCI']
13 # sparse the Hamiltonian and cluster operators using myQLM-fermion tools obtained from MoleculeFactory, which
    explicitly are:
14 hamiltonian_sparse = hamiltonian_jw.get_matrix(sparse=True)
15 cluster_ops_sparse = cluster_ops.get_matrix(sparse=True)
16 # reference_ket and hf_init_sp can be obtained from class MoleculeFactory():
17 reference_ket, hf_init_sp = MoleculeFactory.get_reference_ket(hf_init, nbqubits, 'JW')
18 # when all these parameters are satisfied, then fermionic ADAPT-VQE function is:
19 fermionic_adapt_vqe(cluster_ops, hamiltonian_sparse, cluster_ops_sparse, reference_ket, hf_init_sp, cluster_ops_jw,
    hf_init_sp, n_max_grads, fci, optimizer, tolerance, type_conver = type_conver, threshold_needed =
    threshold_needed, max_external_iterations = max_iterations)

```

`fermionic_adapt_vqe()` calls internally other functions allowing the execution of the steps from 4th to 7th given in subsection 2.4: (1) prepare the trial state through `prepare_state()`; (2) compute analytically the commutator between the hamiltonian and the fermionic operator through `compute_gradient()`; (3) collect and arrange the gradients in a list from maximum to minimum (with avoiding the zeros) through `sorted_gradient()`; (4) if the norm is less than the ( $\epsilon$ ), the program exits returning

<sup>3</sup>We use the function `count()` from Open-VQE to evaluate the gates from the final optimized circuit, among which are the CNOT gates. We count them with the following based condition: If the optimized parameter associated with the full cluster operator `cluster_ops_jw` is less than a certain threshold equal to  $10^{-7}$ , we omit it from the list, which means that the suppressed operators will not be included in the mapping into circuit, and thus the CNOT gates coming from the suppressed operators are not counted.

the generated values, else it will continue calculating the maximum gradient(s) of operator(s) depending on the number of maximum gradient in the input, after that, we append the operator(s) associated with their parameter(s) to the left of the previous trial state (step (1)) during which we apply VQE using function `ucc_action()`, which is described above in order to optimize the parameter(s) until satisfying the threshold's condition; This function returns: (i) the number of classical parameters for the final ansatz, (ii) the number of CNOT gates in the ansatz circuit, (iii) number of other gates, (iv) list of optimized energies corresponding to external iterations and (v) energy subtracted from the full configuration interaction (FCI).

The qubit ADAPT sub-module is globally similar to the fermionic ADAPT in terms of the code structure, some key steps are different and makes it unique in its nature. Those steps can be summarized in the following sequence: (i) we use qubit pool generators (using `QubitPool`) instead of fermionic ones; (ii) the preparation of the trial state is different from the fermionic Adapt one; (iii) the gradients calculation is not the same. It returns the same properties as that of fermionic ADAPT-VQE.

## 5 | SYSTEMATIC BENCHMARKING OF THE PERFORMANCE OF THE VERSIONS OF UCC AND ADAPT-VQE ON SEVERAL MOLECULES USING THE OPEN-VQE PACKAGE

In this section, we performed numerical estimations of ground state energies by means of Open-VQE, more specifically, by using the VQE-UCC-family and ADAPT-VQE modules. This was done for a range of molecules which require from 4 to 24 qubits to be treatable with quantum computing (see Figure 4). We perform only noiseless simulations in order to minimize computational runtime and all simulations were performed on TotalEnergies in-house HPC architecture<sup>4</sup>. We validate our results by comparing some of them with other works obtained with similar methodologies.

For each numerical simulation in the UCC-family or ADAPT-VQE modules, we use the following common functions implemented in Open-VQE to calculate: (i) the molecular orbital integrals using the PYSCF package with the STO-3G, 6-31G and cc-pVDZ basis sets; (ii) the molecular Hamiltonian mapping which is obtained by applying the Jordan-Wigner transformation; (iii) the circuits simulated which are based on the CNOT staircase method, except for QUCCSD version for which we use the two circuits which represent the single and double qubit evolutions (see Figure 1 and 2 in<sup>69</sup>, respectively). We used the `scipy.optimize` library for optimization.

We organize the presentation of our work on molecular simulations using Open-VQE into three main subsections: (i) subsection 5.1 that displays the timings of the QLM simulator for constructing the UCCSD ansatz on a simulator as well as for obtaining the expectation value of the electronic structure Hamiltonian for a set of molecules (STO-3G basis set) ranging from 4 to 24 qubits. (ii) subsection 5.2, dedicated to the UCC-family module, it describes the performance of UCCSD-VQE for H<sub>6</sub> with the STO-3G basis set and for LiH using 6-31G basis set with different sizes of active spaces. Then we focus on H<sub>6</sub> at a single geometrical arrangement to show how close do different optimizers come to the chemical accuracy<sup>5</sup> and how many CNOT gates they require to achieve such an accuracy. We also discuss different ways of choosing the initial wavefunction such as the random guess and Møller-Plesset wavefunction in second order. Secondly we extend our calculations to a larger set of molecules and all considered using the STO-3G basis set. Some computations use a full space and some others include active space selections, in order to compare the chemical accuracy obtained from three different UCCSD: regular UCCSD, UCCSD without the Z-Pauli terms and QUCCSD ansatze. We then compare the results with those obtained from CCSD, CCSD(T), CISD and CIPSI classical methods. Since CIPSI is not a common known method unlike the other three methods, we briefly introduce its definition as follows: the Configuration Interaction using a Perturbative Selection made Iteratively (CIPSI) wave-function is a truncation of the Full Configuration Interaction (FCI) wave-function where the determinant are selected regarding a perturbative selection. The method has been developed since a few decades (see some references in the introduction of<sup>88</sup>) and it is well described in<sup>89,90</sup>; (iii) subsection 5.3 that uses the ADAPT-VQE module. It describes the comparison between the fermionic and qubit ADAPT-VQEs in terms of chemical accuracy by benchmarking the three molecules H<sub>4</sub>, LiH and H<sub>6</sub>, in the STO-3G orbital basis set by assuming a full space selection approximation in each molecule. All CNOT number estimations are obtained using the CNOT staircase circuits. Then, using the fermionic ADAPT-VQE sub-module, we simulated several other molecules using a larger number of qubits and different basis sets assuming full space selection. Such computations were performed in order to demonstrate the capacity of our sub-module code functions to perform larger calculations and to reach chemical accuracy despite the increase

<sup>4</sup>The server we used in our calculations has the following properties: linux machine named "skelling", with 162 cores, each core containing 2 threads. A total memory is 3 094 000 MiB.

<sup>5</sup>For a given basis set, according to Wikipedia, the standard chemical accuracy is 1 kcal/mol which is around  $1.59 \times 10^{-3}$  Hartree. This accuracy represents the error difference between the predicted energy and FCI energy. We use this value as a standard reference in all our results.

of the molecule sizes. Using the same sub-module we also tested several molecules with active space selections to compare the efficiency of fermionic ADAPT-VQE in the context of such active space approximations.

Next we describe how the Qubit-ADAPT-VQE sub-module works through choosing different types of qubit pools, each with a different size. To do so, we study the  $H_4$  molecule using STO-3G basis set. Finally we introduce a brief Table summarizing the comparison of UCC-family methods involving the fermionic excitations (UCCSD and UCCGSD) and fermionic ADAPT-VQE method in several molecules in terms of number of parameters, CNOT counts, chemical accuracy, and computational time.

## 5.1 | Simple UCCSD ansatz: Representative computational performances with Open-VQE

To illustrate the performances of our Open-VQE package on CPUs, we chose to use a standard laptop<sup>6</sup> to evaluate the time to solution required to perform two operations that are common to most of the variational algorithms: (i) the application of the ansatz; (ii) the computation of the expectation value of a molecular Hamiltonian or another observable. Examples of such operations are: the implementing of a Hardware efficient circuit ansatz, or a unitary coupled cluster ansatz; Observables are for example the electronic structure Hamiltonian, a commutator operator, Pauli string terms etc, which can be applied by either of these ansatze to measure their expectation value. As a test, we chose here the UCCSD method to evaluate the timing associated to various computations. It is important to note that, in practice, for the particular case of the simple UCCSD, Open-VQE and the native QLM timings are identical, where QLM simulator used is from QLM version 1.2.1. To measure such timings, we conducted benchmarks with a set of molecules using Open-VQE in the STO-3G basis set ( $H_2$ ,  $H_4$ , LiH,  $H_2O$ ,  $NH_3$ ,  $CH_4$ , CO, HCN, and  $C_2H_2$ ). Figure 4 (a) displays the timings associated to the generation of a state-vector corresponding to the UCCSD ansatz (see Eq. 10) from Open-VQE. The computational cost for this generation grows sub-exponentially with the number of qubits. We observe that the package can compute the UCCSD wavefunction within less than a second for a molecule requiring 4 to 12 qubits, between a second and 10 seconds for molecules associated to a 14-20 qubits range and up to few minutes for larger molecules (22-24 qubits). Figure 4 (b) represents the timing cost for measuring the expectation value of the JW tranformed Hamiltonian (see Eq. 4) of each of these molecules using UCCSD ansatz. This measurement increases linearly with the number of qubits and it is done by using the UCCSD circuit together with the "Job" class which will be submitted to QPU to obtain the expectation value. The process is described by the code function called `UCC_action()` which can be found in section 4. We observe that the computational cost of performing the measurement increases exponentially with the number of qubits. In particular, we notice that molecular systems up to 14 qubits like  $H_2O$  (10 electrons) using Open-VQE, can be performed in a second for a UCCSD circuit. This circuit involves 12,240 CNOT gates and 1,083 Pauli strings, as shown in Figure 4 (c). This Figure also shows the details of the number of CNOT gates and Pauli strings associated to each molecule.

## 5.2 | UCCSD: active space selections, MP2 pre-screening, Influence of the optimization method and comparison with classical methods

### 5.2.1 | Testing active space selections

We test active space (AS) selection approach by simulating  $H_6$  linear geometry type within STO-3G basis set and LiH within 6-31g basis set, for a range of bond lengths for both molecules. For  $H_6$  molecule, which has a Hilbert space spanned by 12 Hartree Fock orbitals, 6 occupied and 6 virtual (i.e., unoccupied) we choose two different active spaces: (i) First 2 spin orbitals where the lowest energies are always filled and 2 spin orbitals where the highest energies are always empty, as these 4 spin-orbitals are not considered in the active space selection, the system consists of 8 active spin orbitals with 4 active electrons which means 8 qubits Hamiltonian; (ii) when we consider that only the first two spin-orbitals are always filled, the system has then 4 active electrons and 10 spin-orbitals corresponding to 10 qubit Hamiltonian. Figure 5 (a) shows the error of ground state energies of  $H_6$  molecule at different dissociation profiles, with different sizes of the active spaces ranging from a minimum 8 qubits to the full space 12 qubits. This error corresponds to absolute value of VQE-UCCSD results substracted from FCI energy. By increasing the active space from 8 to 10 qubits, we observe only few improvements of accuracy and both sizes are still far from approaching the chemical accuracy (see the blue line which was set at  $10^{-3}$  Ha). However in the full space case, the VQE results approach the chemical accuracy before a bond length equal to 1.5 Å. Interestingly, for bond length  $\geq 1.5$  Å, even with full space, the error deviates well beyond the chemical accuracy but it seems to be curving again toward the blue line beyond 3.0 Å. This error means that triple excitations are probably required. A comparable results to our findings for  $H_6$  can be seen

<sup>6</sup>laptop properties are: Intel(R) i5-10310U, Clock speed 2.21 GHz processor, OP windows 10.

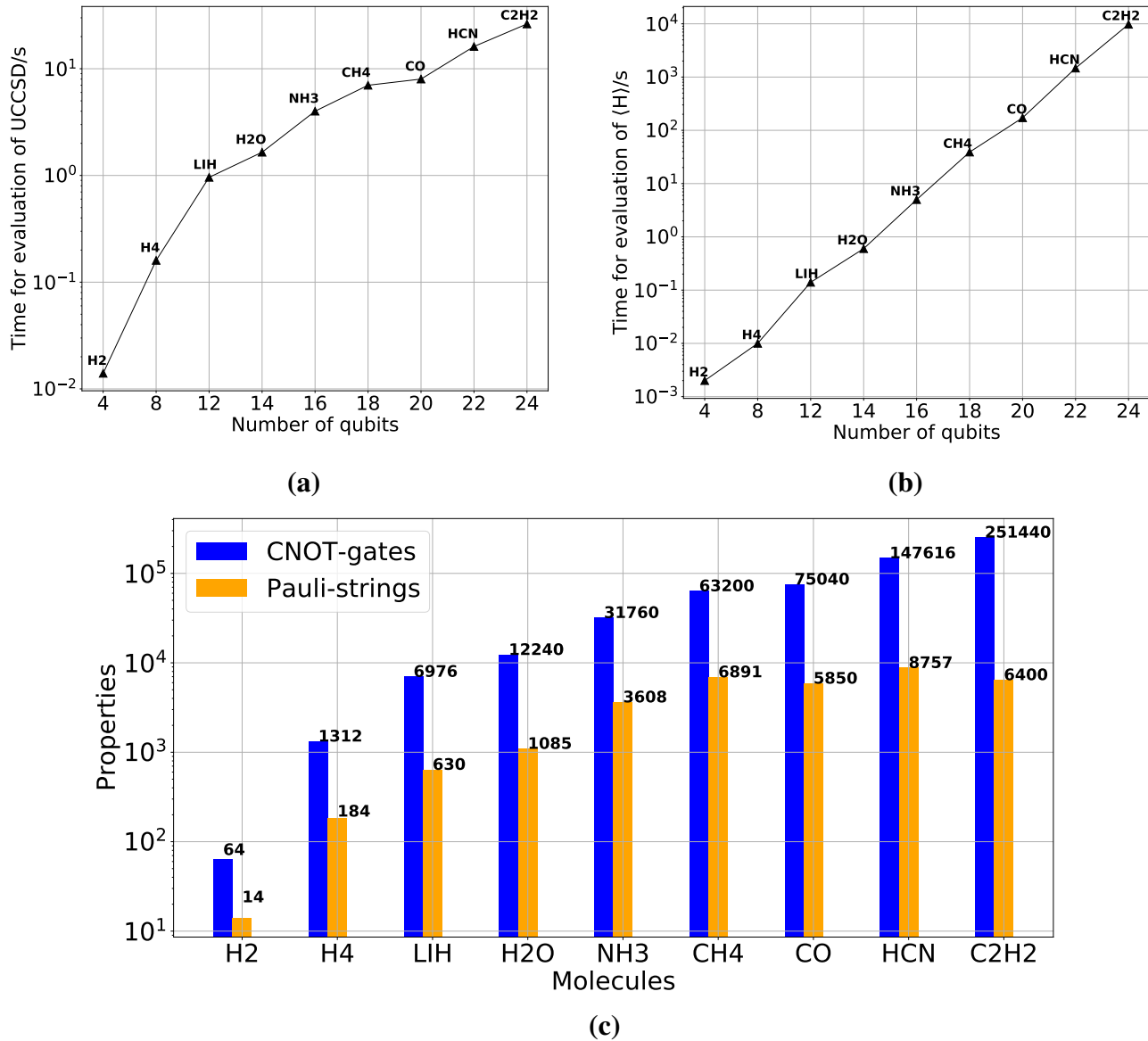


**FIGURE 4** Panel(a): timings for the application of a UCCSD circuit by Open-VQE while increasing the number of qubits. Panel (b): timings for the evaluation of increasing size molecular Hamiltonians (summed over Pauli strings and using using JW transformation) for the following molecules: H<sub>2</sub>, H<sub>4</sub>, LiH, H<sub>2</sub>O, NH<sub>3</sub>, CH<sub>4</sub>, CO, HCN, C<sub>2</sub>H<sub>2</sub>. Panel (c) shows the number of CNOT gates required to complete the UCCSD circuit and the number of Pauli strings in the Hamiltonian. All cluster amplitudes in the UCCSD circuits were initialized to 0.01.

in Figure 7 of<sup>51</sup> but researchers only consider the non-active case there. Figure 5 (b), shows the same energy profile but for LiH molecule. Using the 6-31G basis set, LiH has a Hilbert space spanned by 22 HF orbitals, 4 occupied and 18 virtual (i.e., unoccupied). But five active space selections are chosen, leading to 4, 6, 8, 10 and 12 qubit Hamiltonians. For all choices of active spaces here, the error decreases steadily as the the bond length increased. The 10 and 12 qubit Hamiltonians are below the chemical accuracy for bond length  $> 1.0\text{\AA}$ , while the largest deviation measured is in the intermediate bond lengths range between 1 and 2.4  $\text{\AA}$ . Interestingly, for the 8, 10 and 12 qubits results fall within a narrow range, at bond length before 1.0 and at bond length beyond 2.2  $\text{\AA}$ . Surprisingly, we noticed some jumps in the accuracy for the three cases 6, 8 and 10 qubits at some bond lengths, for example around 2.2  $\text{\AA}$ . A similar analysis has been made in<sup>66</sup> for two different molecules than ours, by

changing the number of qubits in different basis set: (6-31G) in  $\text{H}_2$  and (STO-3G) in  $\text{H}_2\text{O}$ . In particular they observed similar jumps we also observed for  $\text{H}_2\text{O}$  at intermediate range, which as mentioned there it might correspond to geometries close to the so-called Coulson-Fisher point where spin-symmetry breaking can occur<sup>91</sup>.

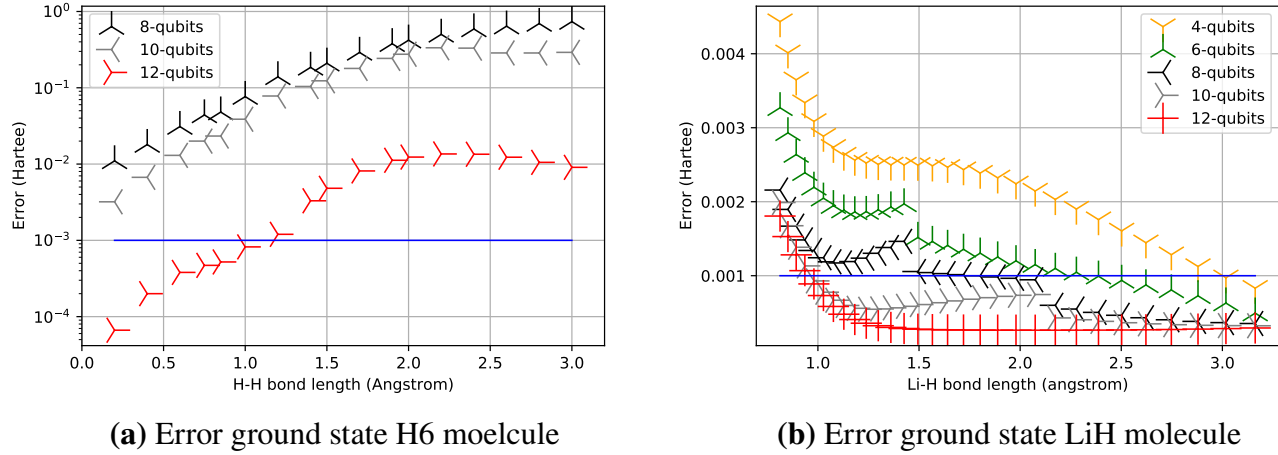


**FIGURE 5** VQE results for the  $\text{H}_6$  molecule using the STO-3G basis set (a) and for LiH with the 6-31G basis (b). The dissociation profile is showed, using different active space selections and are calculated by using the first order trotterization UCCSD ansatz. The size of qubits represents the number of active spin-orbitals. The blue line indicates the chemical accuracy.

### 5.2.2 | Influence of the optimization method in the UCCSD-VQE performance for $\text{H}_6$ at $r=1.0 \text{ \AA}$

After showing the performance of UCCSD-VQE in terms of active space selection and MP2 pre-screening approaches, we show the benefits that Open-VQE can obtain (see Figure 5 ) through using active space selection. Indeed, such a technique allows to approach a similar accuracy as those reached by using a full space at certain bond lengths, even with a smaller number of qubits. Furthermore, in order to test for the usefulness of using MP2 guesses in VQE-UCC algorithm, we choose the  $\text{H}_6$  molecule associated to the STO-3G basis set at a bond length of  $r = 1.0 \text{ \AA}$  using a full space. We calculated UCCSD-VQE energies using six different optimizers, namely COBYLA, BFGS, SLSQP, CG, Powell and Nelder-Mead and with three different initial guesses: (i) random, where random values are chosen uniformly in the interval  $[0.0, 1.0]$ ; (ii) fixed-value of 0.001; (iii) MP2 guesses. In Figure 6 we compare the effects of these initial guesses on the VQE optimization based on three criteria: (i) the number of function evaluations required for convergence in Figure 6 (a); (ii) the error of energy corresponding to VQE energy subtracted from the FCI energy solution in Figure 6 (b); (iii) the number of CNOT gates needed for completing a circuit after final optimization in Figure 6 (c). From Figure 6 (a) we observe that the CO YLA and Nelder-Mead methods require a high number of function evaluation ( $> 30000$ ) for VQE performance when the parameters are chosen randomly. Conversely, the other optimizers (BFGS, SLSQP, CG and Powell) requirements appear smaller number with less function evaluations (about 3000 up to 10000) until reaching convergence. In practice, Nelder-Mead is clearly not adapted to this case where it exhibits high energy errors beyond 0.1 Ha, as shown in Figure 6 (b). The COBYLA method brings better accuracy than SLSQP, which nevertheless needs a smaller number of function evaluations. COBYLA is known to have a better ability to explore the energy than SLSQP. The other optimizers BFGS, CG and Powell bring comparable results between  $10^{-1}$  and  $10^{-2}$  Ha. On the other hand, for the 0.001 fixed-value and MP2 initial guesses methods- COBYLA, BFGS, SLSQP, CG and Powell converge well to almost the same minimum of accuracy, which is under than  $10^{-3}$  Ha.

In general, the number of evaluation changes depending on the type of the optimizer: some optimizers require the estimation of the gradients (BFGS, SLSQP and CG) and some belong to the class of gradient-free optimizers (COBYLA, Powell, Nelder-Mead). From Figure 6 (a) it is clear that gradient-based optimizers (BFGS, SLSQP and CG) require less function evaluations as compared to gradient-free ones (COBYLA, Powell, Nelder-Mead). This is true for every optimizer and choice of initial parameters except for "random" where the Powell optimizer requires less function evaluations as compared to SLSQP and

BFGS. We hypothesise that this behaviour is due to the fact that the random guess of the initial parameters was closer to the optimum in the case when Powell optimizer was used. However, this advantage in using gradient-based as opposed to gradient-free optimizers might not remain when executing algorithms on actual hardware where shot noise, relaxation and dephasing somewhat randomize the optimization landscape, making the estimation of gradients, especially fine ones, more challenging. The energy error follows a somewhat similar trend (subfigure (b)). Figure 6 (c) shows that by using `count()` function found in Open-VQE package, MP2 guesses lead to reduce the CNOT gates in the final circuit when using BFGS, SLSQP, CG and Powell methods. The CNOT gates are reduced by about a half compared to COBYLA or Nelder-Mead. Moreover MP2 guess shows better reductions in CNOT gates when compared to random or 0.001 fixed-value guesses. Similar analysis and comparisons between different optimizers and initial guesses showing the importance of using MP2 guess is studied for  $H_4$  molecule, there not only linear geometry path has been tested but also rectangular and trapezoidal paths<sup>35</sup>, showing that when MP2 guess is used, a smaller number of function evaluations is required, regardless which path of geometry is considered.

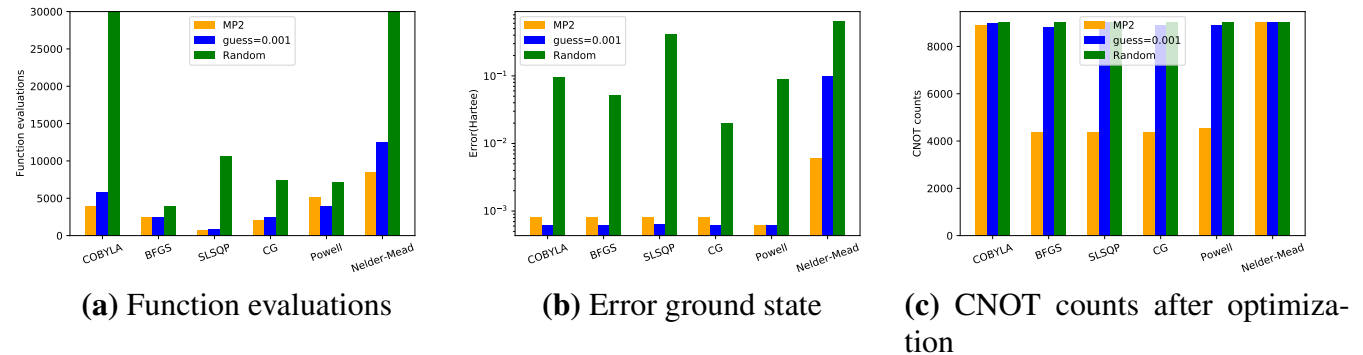


**FIGURE 6** Basic VQE-UCCSD performances applied to the  $H_6$  linear system studied using six different optimization methods (COBYLA, BFGS, SLSQP, CG, Powell and Nelder-Mead) and three distinct starting guesses for the parameters (chosen randomly from interval  $[0.0, 1.0]$ ). (Random), all parameters were fixed at 0.001 (0.001) and used MP2 amplitudes (MP2). We compare the number of function evaluations required for convergence (Final accuracy in the optimization set as  $10^{-4}$ ) (panel (a)), the error in the final energy with respect to the FCI energy (panel (b)), the number of CNOT gates after optimization (panel(c)). The scale of function evaluations is truncated at 30000 to enable comparisons. We remind also that we choose a tolerance of  $10^{-7}$ . In practice, if the parameters values appear below this condition then the operators associated to these parameters are omitted from the final UCCSD wave function.

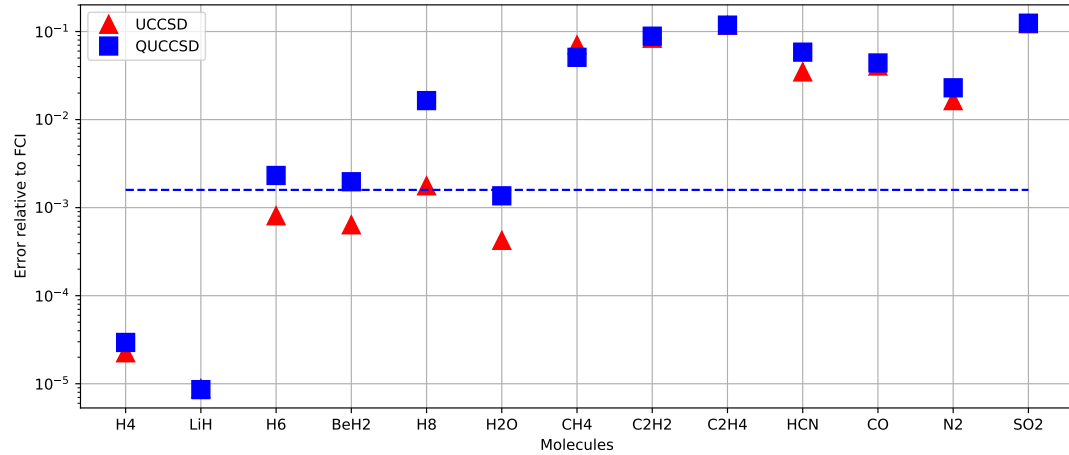
### 5.2.3 | Estimation of UCCSD and QUCCSD accuracies compared to classical methods and of the required quantum resources for a range of molecules in STO-3G basis set

Following our previous discussion, we used the UCCSD and QUCCSD methods to build ansatze and MP2 initial as guesses. UCCSD and QUCCSD circuits are implemented in Open-VQE based on the CNOT staircase method and so are QUCCSD circuits while we are using the efficient circuits introduced in<sup>69</sup>. The optimization is performed with the BFGS algorithm as the maximum number of function evaluations was fixed at 50,000. To compare the resulting UCCSD and QUCCSD energies we calculated the ground state energies of the same molecules using the following four classical methods: CCSD, CCSD(T), CISD and CIPSI. The first three methods were carried out by using the Gaussian software package<sup>92</sup>, while CIPSI was carried out by using the Quantum Package (QP)<sup>93</sup>. We also computed the FCI (for STO-3G) energy using the functions implemented in the QLM library based on PYSCF package. We choose the following set of molecules,  $H_4$ , LiH,  $H_6$ ,  $BeH_2$ ,  $H_8$ ,  $H_2O$  whose geometries are near equilibrium and are detailed in the `MoleculeFactory` class in  $(x, y, z)$  format in Open-VQE. We choose other larger size molecules  $CH_4$ ,  $C_2H_2$ ,  $C_2H_4$ , HCN, CO,  $N_2$  and  $SO_2$ , which we also present in the same format in `MoleculeFactory`. We took the geometries of these near equilibrium larger molecules from the NIST Diatomic Spectral Database<sup>94,95,96,97</sup>. All these molecules we consider have a singlet spin ground state. Moreover we consider all these molecules using full space selections when we apply the three methods: CCSD, CCSD(T) and CISD. However, it is not the case when we calculate UCCSD- and

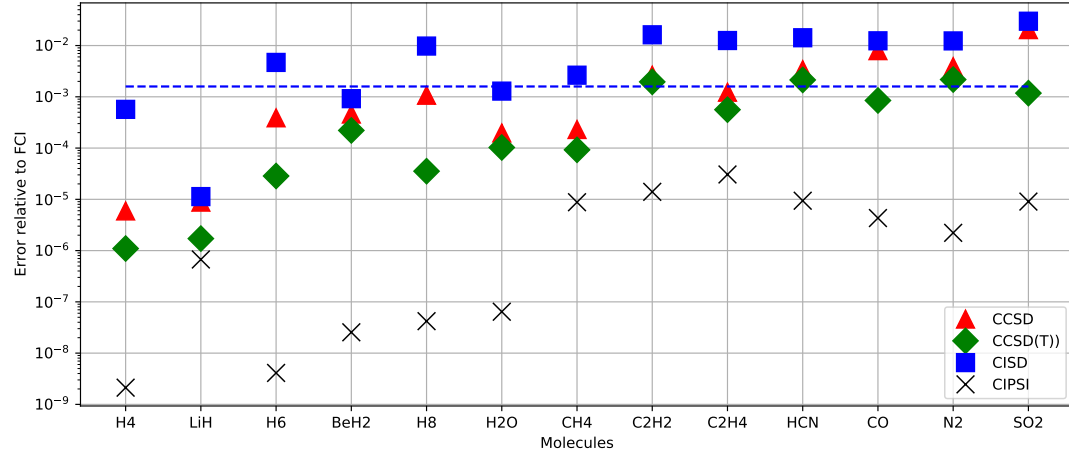
### QUCCSD-VQE:

(i) we consider full space selection for molecules ranging between 8 and 20 qubits, which are,  $H_4$  (8 qubits),  $LiH$  (12 qubits),  $H_6$  (12 qubits),  $H_2O$  (14 qubits),  $BeH_2$  (14 qubits) and  $H_8$  (20 qubits); (ii) we consider (AS) selection for molecules which are represented by more than 20 qubits due to the limitations of QLM simulator in our server (see section 3). So for the following molecules we choose:  $CH_4$  (AS( $6\eta, 10N_A$ )) i.e (10 qubits),  $C_2H_2$  (AS( $8\eta, 12N_A$ )) i.e (12),  $C_2H_4$  (AS( $4\eta, 14N_A$ )) i.e (14 qubits),  $HCN$  (AS( $6\eta, 14N_A$ )) i.e (14 qubits),  $CO$  (AS( $6\eta, 12N_A$ )) i.e (12 qubits),  $N_2$  (AS( $8\eta, 12N_A$ )) i.e (12 qubits), and  $SO_2$  (AS( $8\eta, 12N_A$ )) i.e (12 qubits). In Figure 7 (a), we present the results for the UCCSD and QUCCSD ansatze. These numerical values are obtained taking the absolute values of the subtraction of the UCCSD and QUCCSD estimated energy from the corresponding FCI energy. As is seen in Figure 7 (a) Comparing ansatz performance of UCCSD to QUCCSD, we observe different cases for molecules in case of full space selections: (i) in molecules ( $H_4$  and  $LiH$ ), the QUCCD achieves the same level of accuracy compared to the UCCSD; (ii) in molecules ( $H_6$ ,  $BeH_2$  and  $H_2O$ ) there is a difference in the error where QUCCSD performs worse compared to UCCSD, moreover, QUCCSD is still around the chemical accuracy level on these three molecules. In  $H_8$ , the error increased by around one order of magnitude (i.e from  $10^{-3}$  up to  $10^{-2}$  Ha) and is above the chemical accuracy. The reason for these error changes is that the QUCCSD ansatze fail to recover the correlation effects that become stronger at certain bond lengths especially when the system qubit size increases (i.e. like for the 20 qubits  $H_8$  system). Now for molecules within the active space selection, the QUCCSD ansatz performs as accurately as UCCSD. This means that within this size of qubits, the removal of parity terms in excitation operators may not affect accuracy of the QUCCSD method compared to UCCSD. This is consistent with previous results obtained in reference<sup>51</sup> where the accuracy reached by QUCCSD was found comparable to that obtained with UCCSD for a test set of molecules including  $H_4$ ,  $H_6$ ,  $BeH_2$ ,  $H_2O$  and  $N_2$  at similar bond lengths. Such data tend to show that despite the sole inclusion of single and double excitations, QUCCSD can approximate electronic wavefunction almost as accurately as UCCSD while not being as reliable. It can be particularly noticed in the cases of strongly correlated systems within full space ( $H_8$ ).

Figure 7 (b), displays a comparison between the CCSD, CCSD(T), CISD and CIPSI classical methods, it appears that CIPSI results bring the most accurate results for all the molecules presented and by at least one order of magnitude from CCSD(T). Comparing UCCSD-VQE Figure 7 (a) to the classical methods in Figure 7 (b), we find similar order of magnitude for CCSD and better than CISD, for molecules ( $H_4$ ,  $LiH$ ,  $H_6$ ,  $BeH_2$ ,  $H_8$  and  $H_2O$ ). Within these molecules CCSD(T) is better. For molecules calculated within active space selection, we clearly find that classical methods, mainly CCSD(T) and CIPSI, bring better accuracy, due to the fact that core orbitals are not frozen in these cases. Interestingly, some molecules like  $C_2H_4$ ,  $CO$  and  $SO_2$  as is seen in Figure 7 (a) still approach the accuracy of classical methods mainly CISD and CCSD. However CISD and CCSD are also far from the chemical accuracy which CCSD(T) does. This shows that apart from active space selection approach, the triple excitations for large molecules is required to perform UCCSD(T) or even the UCCSDT(Q). These observed results show that despite the fact that the unitary coupled cluster works very well within active space selection for some molecules, this is not definitive. The results could probably be improved with more qubits/larger active space selection and/or adding triple excitations. A future work will provide enhanced accuracy by improving the QLM simulator (increasing the number of qubits). It is worth pointing out that an analysis for some molecules comparing the classical methods to UCCSD was previously studied in references.<sup>98,99</sup>



(a) UCCSD and QUCCSD methods.



(b) CCSD, CCSD(T), CISD and CIPSI methods.

**FIGURE 7** Error,  $(E - E_{FCI})$  in Hartree, from (a) UCCSD and QUCCSD, (b) CCSD, CCSD(T), CISD and CIPSI method calculations for a range of molecules with near equilibrium geometries. The basis set is STO-3G and all molecules are within a spin singlets state. (c) CNOT gates counts for UCCSD and QUCCSD after optimization (using MP2 Guess). Molecules CH<sub>4</sub>, C<sub>2</sub>H<sub>2</sub>, C<sub>2</sub>H<sub>4</sub>, HCN, CO, N<sub>2</sub> and SO<sub>2</sub> are within active space selections (see text above). The dashed blue line indicates the chemical accuracy.

In Figure 8, we roughly estimate the number of CNOT gates from UCCSD and QUCCSD ansatz for all the molecules listed above. We are interested in counting these gates because they are now the most critical required recodesources in the NISQ devices. Using our code function to count CNOT gates, we obtained very good count reduction. For example, for LiH, the number of CNOT gates went from 6976 to 4720 with UCCSD ansatz (before and after the initial MP2 guess and subsequent optimization) and to (1112) with QUCCSD ansatz. For BeH<sub>2</sub> molecule, from 18208 to 6368 with UCCSD (before and after the initial MP2 guess and subsequent optimization) and to (2592) with QUCCSD. We notice that in some molecules the CNOT count is reduced by around one-half between UCCSD and QUCCSD ansatzes.

Furthermore, for some other molecules within the active space selection approximation such as C<sub>2</sub>H<sub>2</sub>, SO<sub>2</sub>, CH<sub>4</sub>, and C<sub>2</sub>H<sub>4</sub>, the final CNOT counts with UCCSD and QUCCSD are about the same. We can conclude that QUCCSD exhibits lower gate

counts, as compared to QLM's UCCSD, due to its qubit evolutions construction. These CNOT gates counts with UCCSD and QUCCSD have been previously studied for LiH, H<sub>6</sub> and BeH<sub>2</sub> in<sup>70</sup>(see Table 3.1 in Chapter 4).

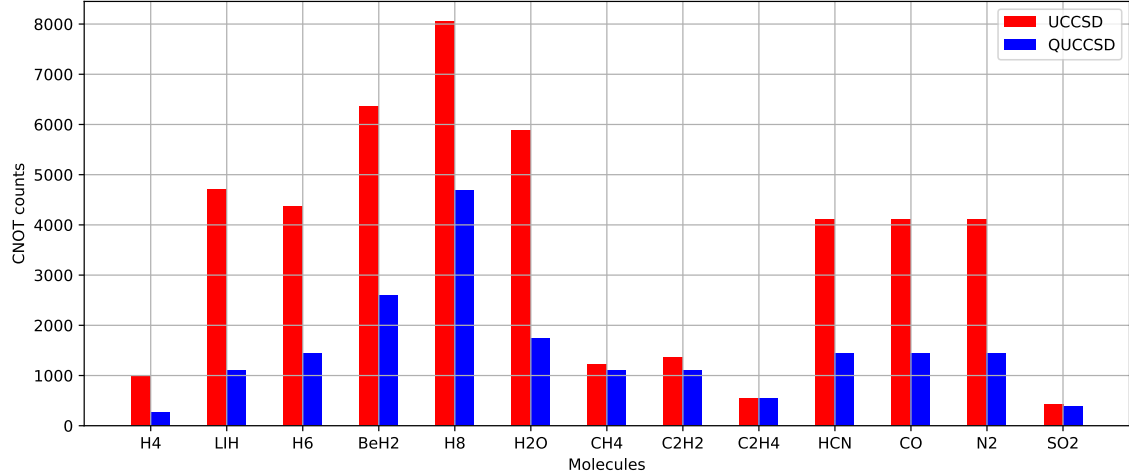


**FIGURE 8** CNOT gates counts for UCCSD and QUCCSD after optimization (using MP2 Guess), such that optimized parameters  $\leq 10^{-8}$  are not counted.

### 5.3 | Performance of ADAPT-VQE module in Open-VQE

#### 5.3.1 | Two implementations of fermionic ADAPT-VQE and qubit ADAPT-VQE

In Figure 9, we represent the energy convergence for LiH, H<sub>4</sub> and H<sub>6</sub>, obtained with the fermionic ADAPT-VQE and qubit ADAPT-VQE approaches. The three molecules are at bond lengths  $r_{\text{Li-H}} = 1.45\text{\AA}$ ,  $r_{\text{H-H}} = 0.85\text{\AA}$ , and H<sub>6</sub> at bond distance  $r_{\text{H-H}} = 1.0\text{\AA}$ , respectively. All convergence plots are terminated when the norm value is below the threshold  $\epsilon$  (see Eq. 17 in section 2.4), which is between  $10^{-3}$  and  $10^{-4}$  for fermionic ADAPT-VQE, and between  $10^{-3}$  and  $10^{-6}$  for qubit ADAPT-VQE, depending on the molecule. Since we find SLSQP and BFGS optimizers behave comparably for energy convergence (after using MP2 initial guess) as is noticed in Figure 6, we used SLSQP optimizer for fermionic ADAPT-VQE and the BFGS optimizer for qubit ADAPT-VQE. The plots in Figure 9 present the two protocols in terms of two important conditions, required to construct an ansatz and to achieve a specific chemical accuracy : (i) the number of iterations (or parameters); (ii) the number of CNOT gates. Figures 9 (a,b,c)- show that the fermionic ADAPT-VQE converges faster than the qubit ADAPT-VQE, requiring systematically fewer number of iterations and thus variational parameters. However as is shown in Figures 9 (d,e,f)- the CNOT counts from the fermionic ADAPT-VQE to reach convergence, are higher by more than one-order of magnitude with respect to qubit-ADAPT-VQE to complete a circuit at a certain level of accuracy for each molecule. Such results make sense with the fermionic ADAPT-VQE approach since the type of operators is spin-complemented pairs (see eqs. A1 and A2). Indeed, the JW transformation of single and double operators will lead to sets of two and eight Pauli strings, respectively, where each Pauli string is a tensor product of Pauli matrices. According to theory, there are four CNOT staircases (for a single excitation) and sixteen (for a double excitation)<sup>68</sup>. The qubit ADAPT-VQE theory (see section 2.4) states that the pool consists of many individual Pauli strings. This means the qubit ADAPT-VQE needs more ansatz elements i.e operators or parameters, to reach convergence. But at the same time, the CNOT counts are much reduced with respect to fermionic ADAPT-VQE. Similar results of CNOT counts, number of parameters and chemical accuracy for fermionic ADAPT-VQE involving LiH and H<sub>6</sub> molecules are presented in Figure 2 of<sup>41</sup>. For LiH we match these results but for H<sub>6</sub> some differences occur since we have gone beyond the  $10^{-3}$  threshold. This has added more parameters to the ansatz and therefore a better accuracy. In<sup>50</sup> (Figure 1) results of fermionic and qubit ADAPT-VQE involving LiH ( $r = 2.0\text{\AA}$ ), H<sub>4</sub> ( $r = 1.5\text{\AA}$ ) and H<sub>6</sub> ( $r = 2.0\text{\AA}$ ) are also comparable to our findings but might be slightly difference because of different geometries in the three molecules, and threshold.

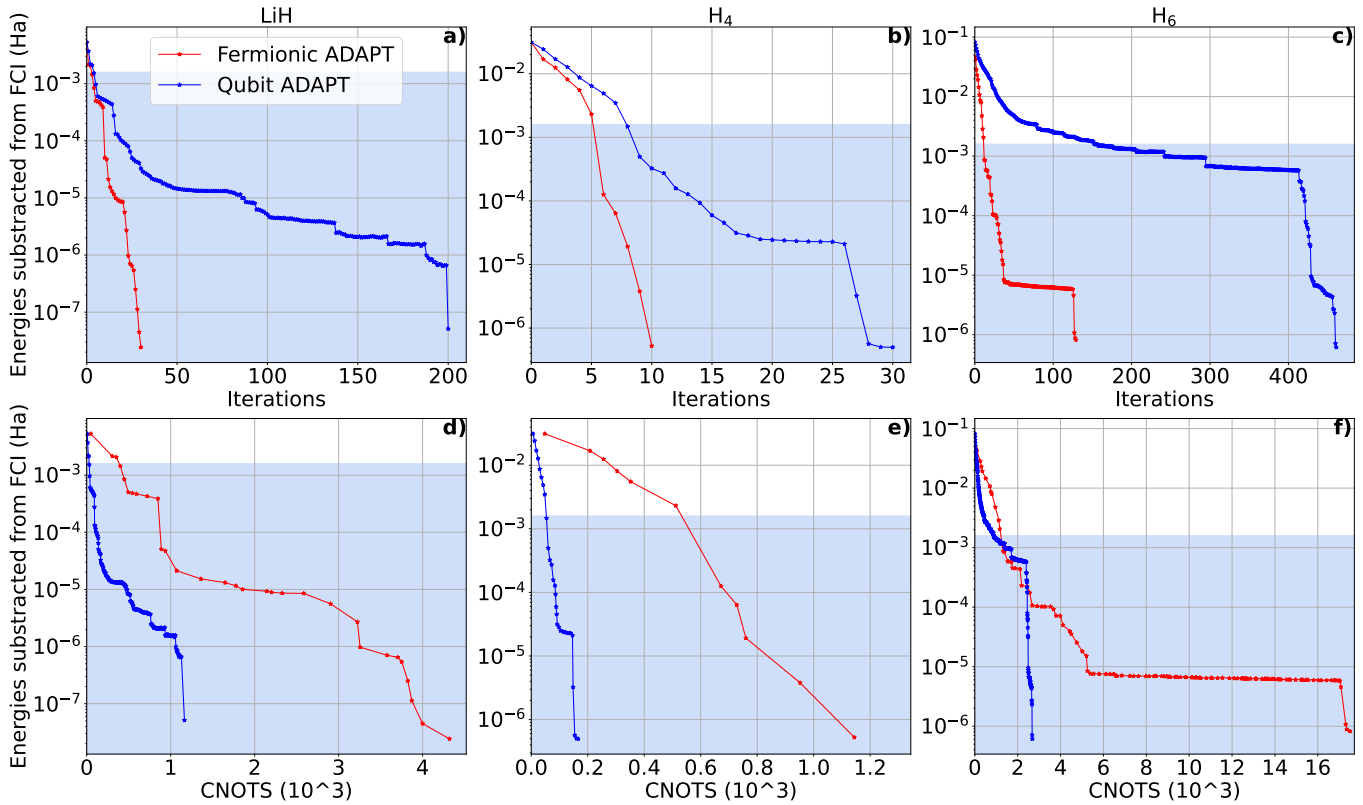


**FIGURE 9** Energy convergence plots for the near equilibrium ground states of LiH,  $H_4$  and  $H_6$  using the STO-3G orbital basis set, at bond distances  $r_{\text{Li-H}} = 1.45\text{\AA}$ ,  $r_{\text{H-H}} = 0.85\text{\AA}$ , and  $r_{\text{H-H}} = 1.0\text{\AA}$ . The red plots are obtained with a fermionic-ADAPT-VQE approach and the blue plots are obtained with qubit ADAPT-VQE. Top panels (a,b,c) present the energy accuracy as a function of the ansatz parameters (note that for both ADAPT-VQE, the number of parameters are the same as the number of operators taken per iteration). Bottom panels (d,e,f) present the energy accuracy as a function of the CNOT count of the ansatz circuit. The blue area corresponds to the chemical accuracy.

### 5.3.2 | Fermionic ADAPT-VQE: simulation several molecules up to 22 qubits, in different basis sets, comparing active and non-active selections

In this subsection, using the fermionic ADAPT-VQE sub-module from open-VQE, we simulate a set of molecules (from 12 qubits up to 22 qubits) without active space selections with different basis sets. These molecules are: (i) with the STO-3G basis set:  $\text{OH}^-$  (12 qubits), HF (12 qubits),  $\text{H}_2\text{O}$  (14 qubits),  $\text{BeH}_2$  (14 qubits),  $\text{NH}_3$  (16 qubits) and  $\text{H}_8$  (20 qubits); (ii) with the 6-31G basis set:  $H_4$  (16 qubits) and LiH (22 qubits); (iii) in cc-pVDZ,  $H_2$  (20 qubits). The goal here is to compare both the fermionic ADAPT-VQE energies of these molecules affected by a  $\epsilon$  threshold value as well and the efficiency of our simulator. Figure 10 (a) shows the energy error convergence plots for the set of molecules controlled by a given value of  $\epsilon$ : (i)  $\text{NH}_3$  and  $\text{H}_8$  ( $\epsilon \leq 10^{-1}$ ), (ii)  $\text{BeH}_2$  ( $\epsilon \leq 10^{-2}$ ); (iii)  $H_4$  and LiH ( $\epsilon \leq 10^{-3}$ ); (iv)  $\text{OH}^-$ , HF,  $H_2$  and  $\text{H}_2\text{O}$  ( $\epsilon \leq 10^{-5}$ ). We also observe in the Figure, that for example  $H_2$  (cc-pVDZ) and  $\text{OH}^-$  or HF (STO-3G) exhibit a precision better than  $10^{-8}$  (Ha) which is not the case for  $H_4$  and LiH (6-31G) since the ADAPT-VQE loop stops at the given threshold (i.e.  $\epsilon \leq 10^{-3}$ ). We also observe from the same Figure that even with  $\text{H}_2\text{O}$ , with the highest number of qubits (14 qubits), stopped at a threshold of  $\epsilon \leq 10^{-5}$ , we obtained a very good accuracy, the error being less than  $10^{-6}$  Ha. It is known from the literature, that as the threshold decreases, the chemical accuracy is improved regardless of the chosen basis set. To illustrate this point (see Figure C3 ), we represent the detailed ADAPT-VQE calculations in  $H_2$  molecule using the cc-pVDZ basis set, showing that controlling  $\epsilon$  at  $10^{-4}$  brings very good accuracy (i.e. around  $10^{-9}$  Ha) with respect to FCI(cc-pVDZ). For some molecules, we realized that some convergence problems might appear at certain levels of accuracy from fermionic ADAPT-VQE especially when the size of molecules gets larger while including enough number of electrons. A similar study has been done for other sets of molecules in<sup>100</sup> where authors used Qiskit's state-vector simulator. They already mentioned the difficulty of fermionic ADAPT-VQE method in reaching certain

convergence especially when  $\epsilon$  gets too small i.e less than  $10^{-4}$ , in this paper it is suggested that choosing several maximum gradients (like 3 or 4) at each iteration instead of one maximum gradient can improve the convergence and reduce the number of iterations. Following this hypothesis, we are currently testing some larger molecular sizes in order to investigate how could the number of iterations, parameters and CNOTs could reduce instead of considering only one maximum gradient per external iteration in the ADAPT algorithm. We also tested the OpenVQE fermionic ADAPT module on a number of molecules using active space selection. The following molecules were simulated: (i) in STO-3G,  $\text{OH}^-$  (10 qubits),  $\text{LiH}$  (10 qubits),  $\text{H}_2\text{O}$  (12 qubits),  $\text{NH}_3$  (14 qubits; (ii) in 6-31G,  $\text{LiH}$  (20 qubits). When we fixed the threshold ( $\epsilon \leq 10^{-3}$ ), we observe in Figure 10 (b) that even with the reduction of qubits by 2 in each molecule, the accuracy is still around and even a bit beyond the chemical accuracy (which we assume to be  $10^{-3}$  Ha). Similarly to the non-active selection case, the threshold value of fermionic ADAPT-VQE must decrease in order to obtain better chemical accuracy. However, a good sign is that with qubit reductions, the fermionic ADAPT-VQE algorithm remains functional. This reduced the number of operators in the pool and thus the cost of gradient measurements. In a near future, we want to test molecules which require high numbers of qubits and to go beyond the STO-3G basis set ( $\text{CO}_2$  or  $\text{C}_2\text{H}_4$ , benzene etc...) using the active space selection approximation. Such benchmarks are intended to check whether the performance of fermionic ADAPT-VQE from the QLM simulator is still working efficiently as the molecule size gets larger, especially with maintaining the level of accuracy.

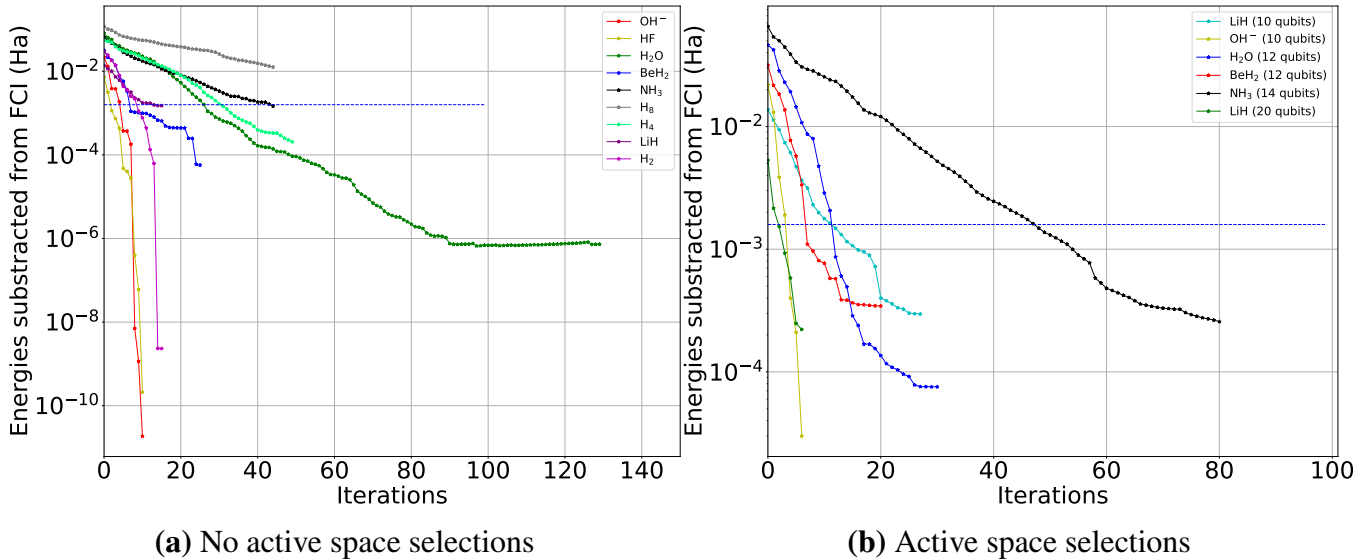


**FIGURE 10** Fermionic ADAPT VQE simulations for a set of molecules ranging between 12 and 22 qubits. Iterations were stopped based on a given norm threshold condition. Subfigure (a) shows the error of energy for a set of molecules that are all assumed with full space selections and the STO-3G basis set for  $\text{OH}^-$ ,  $\text{H}_2\text{O}$ ,  $\text{BeH}_2$ ,  $\text{NH}_3$  and  $\text{H}_8$ , with 6-31G for  $\text{H}_4$  and  $\text{LiH}$ , with cc-pVQZ for  $\text{H}_2$ . Subfigure (b) shows the error of the energy for set a of molecules all assuming active space selections to taper-off 2 qubits for each of the following molecules: in STO-3G for  $\text{OH}^-$ ,  $\text{H}_2\text{O}$ ,  $\text{BeH}_2$ ,  $\text{NH}_3$ , with 6-31G for  $\text{LiH}$ . The dashed blue lines indicate the chemical accuracy.

### 5.3.3 | Qubit-ADAPT: testing several qubit pools

We study here in detail the qubit ADAPT-VQE by providing an example of  $\text{H}_4$  molecule at  $r = 0.85\text{\AA}$ . In this molecule we make different qubit pools choices applying different sizes. We performed such simulations with different pools to test which pool could achieve a satisfying precision with fewest iterations and CNOTs counts, and a reduced computational cost in term of

gradients evaluation. We choose the first qubit pool by breaking down the spin-adapted fermionic operators<sup>7</sup>, obtained after JW transformation and we choose the individual Pauli strings<sup>8</sup> which constructs the pool. Each individual Pauli string has the form

$$Q_m \equiv i\Pi_i p_i, p_i \in X, Y, Z \quad (20)$$

and we named this qubit pool collecting  $Q_m$  as *full*. It is obvious this pool would yield larger sizes because it includes a large number of Pauli strings which consequently lead to a large number of CNOTs. Possible ways to reduce the number of CNOTs and the pool size is by omitting the  $Z$  Pauli terms from *full*, which we named as *full\_without\_Z*. We can further reduce the pool by keeping the first string acting on each combination of spin orbitals named as *reduced\_without\_Z*<sup>9</sup>. Another possibility to test how pool size behaves is to choose one type of the following strings<sup>10</sup> ( $YXXX, XYXX, XXYX, XXXY$ ) and discarding their counter parts<sup>11</sup>. It appears that *reduced\_without\_Z* pool is the same as  $YXXX$  pool operators at least for  $H_4$  but not necessarily for other molecules with larger number of qubits. Randomly selecting operators from ( $YXXX, XYXX, XXYX$  and  $XXXY$ ) and creating a pool mix out of them is named *Random*. Further directions to check the chemical accuracy and the number of iterations from qubit ADAPT-VQE ansatz is to group these Pauli strings into two or four qubit pools. We finally introduce a pool related to  $H_4$  named *symmetry*, introduced in<sup>52</sup> (given in Eq. (11) therein). Very interesting that this pool contains the smallest number of operators<sup>12</sup>, complete and minimal, preserving symmetry to avoid convergence problems. To do this test on our simulator, we use Open-VQE<sup>13</sup> to simulate the  $H_4$  molecule by applying qubit ADAPT-VQE sub-module within the different pool size choices described above. For optimizing the search through the hyper-parameter space of rotations of quantum gates we choose SLSQP algorithm with the energy convergence threshold of  $10^{-13}$  (Ha). Figure 11 (a) presents the energy convergence plots with respect to FCI for each of the qubit pools. We observe that all these pools reach a chemical accuracy better than  $10^{-8}$  Ha. We also observe that Qubit pool  $XXYX$  provides an accuracy above  $10^{-10}$  Ha then it loses accuracy due to convergence problems we observed<sup>14</sup>. Other qubit pools yield an accuracy between  $10^{-10}$  and around  $10^{-12}$  Ha. Even though *full* and *four* pools reach comparable accuracy as that of *symmetry*, we observe no convergence problems with the latter since the *symmetry* pool preserves the *parity* symmetry, which is a property that other pools can miss. Our results are similar to that provided in<sup>50</sup> where some pool reduction simulation studies are analyzed for  $H_4$  and LiH molecules. Concerning the *symmetry* pool, a detailed analysis of this pool for the case of the  $H_4$  molecule is given in Ref.<sup>52</sup>, but researchers there have performed their calculations analytically (i.e the exponential matrix of  $Q_m$  is calculated by using `scipy.linalg.expm(Q_m)` method). Here we use the CNOT staircase method that map the exponential of Pauli strings found in the pool using QLM simulator. A comparison of our results in Figure 11 (a) to Figure 3 (b) found in<sup>52</sup>) illustrates that the QLM produces results similar as those of the analytical calculations. Figure 11 (b) shows the number of CNOT gates, the number of iterations needed to implement the ansatz and the size of each pool.

As is shown from Figure 11 (b), the *symmetry* pool requires higher number of CNOTs and iterations for completing an ansatz compared with some other pools at this level of accuracy. The *symmetry* pool still exhibits the lowest pool size (11 operators) which obviously helps a lot in reducing the cost of gradient energy measurements. Furthermore to construct the symmetry pools we can follow a recent work (see<sup>52</sup>). In this reference,  $H_4$ , LiH (18 operators) and  $BeH_2$  (22 operators) are constructed by freezing one orbital per molecule which reduces the qubits counts: 10 for LiH and 12 for  $BeH_2$  using the STO-3G basis set.

### 5.3.4 | Comparison of fixed-length ansatze with ADAPT-VQE methods

In this subsection we want to determine how many parameters, CNOT-gates, and which energy accuracy is reached by the "fixed-length ansatze" as opposed to the fermionic ADAPT-VQE. To do so, we choose the LiH (1.45 Å) and  $H_6$  (1.0 Å) molecules as benchmarks.

In Figures 7 (a and c) and 10 (a,b,d and f) the attempt to reach chemical accuracy is displayed alongside with the number of CNOTs for both the UCCSD and fermionic ADAPT-VQE. The UCCGSD (see Eq. 12) method remains to be characterized. We

<sup>7</sup>The singlet generalized single and double excitation operators is considered which we already used in Open-VQE.

<sup>8</sup>the individual Pauli string in any qubit pool listed here has an important property: it contains an odd number of  $Y$ s because the fermionic operators are real. To make the final string real, it is multiplied by an imaginary part ( $i$ ), however strings of even numbers of  $Y$ s cannot be considered because they don't affect the energy gradient

<sup>9</sup> $YXXX$  strings comes always the first, because of internal organization from QLM/myQLM library

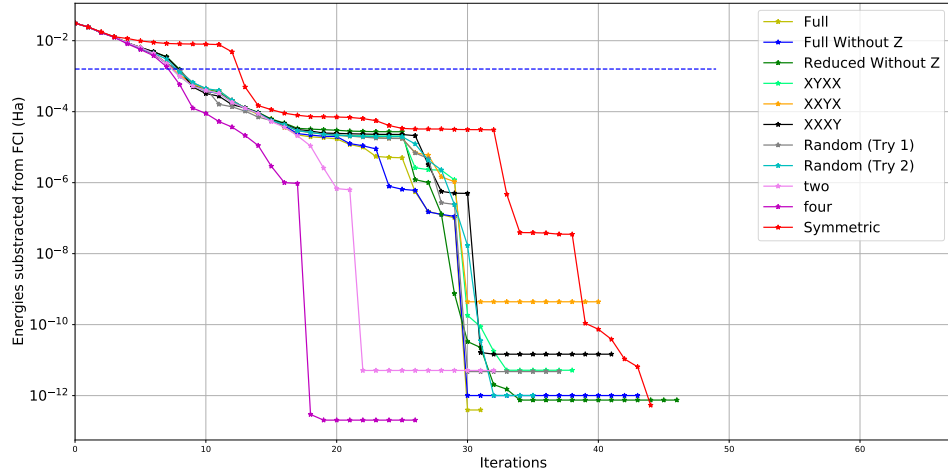
<sup>10</sup>In the Jordan-Wigner transformation spin-up orbitals are mapped to even-numbered states and spin-down orbitals to odd-numbered states. This means that for the case of the single excitations (acts on qubits  $i$  and  $k$ ) we only keep the excitations that satisfy  $i = k \pmod{2}$ , where mod denotes the modulo operation. Similarly, for the double excitations (acts on qubits  $i, j, k, l$ ) we only keep that  $i + j = k + l \pmod{2}$ .

<sup>11</sup>there are pairs of operators that are related by a global rotation, e.g.,  $Y_0 X_1 X_2 X_3$  and  $X_0 Y_1 Y_2 Y_3$ , so that we only need to keep one of them in the pool

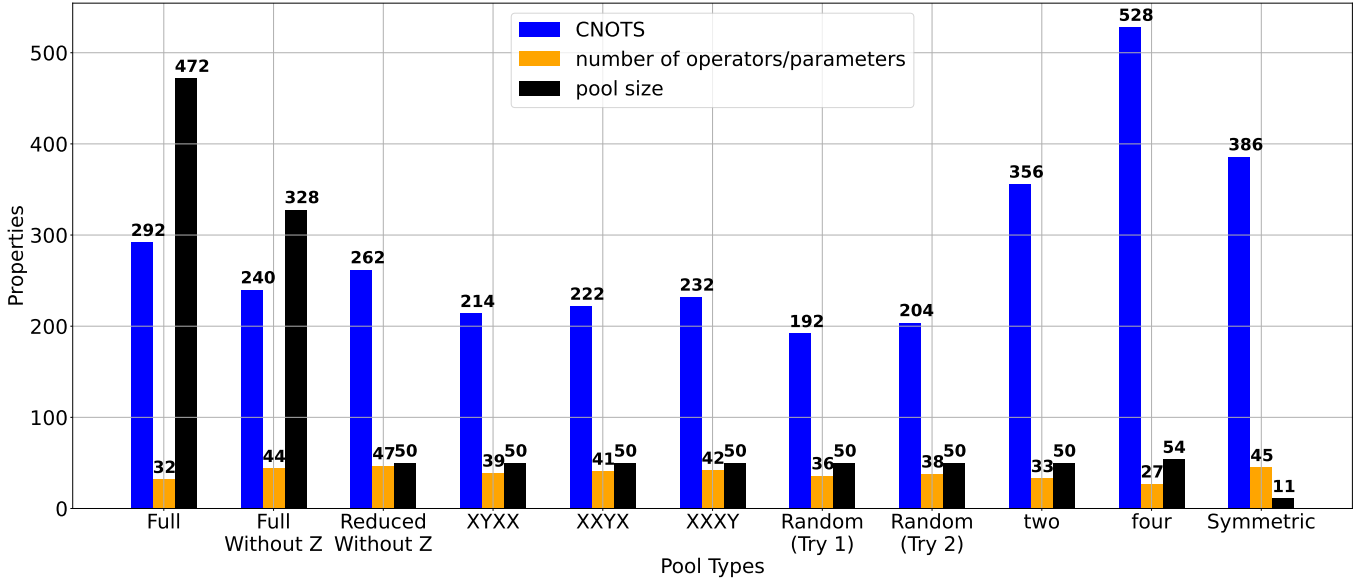
<sup>12</sup>it scales linearly with the number of qubits (i.e  $2n-2$ ) according to<sup>52</sup>, this finding reduces the measurement cost from  $O(n^8)$  to  $O(n^5)$  in case of any molecular problems

<sup>13</sup>all Qubit pools are coded in Qubit Pool python class as discussed in subsection 4 and for the *symmetry* pool we followed the rules mentioned in<sup>52</sup> to classify which pool must be chosen as starters when we perform the loop of iterations

<sup>14</sup>Horizontal straight lines corresponds to poor convergences



**(a)** Error for the ground state energy of the  $\text{H}_4$  molecule (non-frozen: 8 qubits). The dashed blue line indicates the chemical accuracy.



**(b)** Properties of qubit pools

**FIGURE 11** Qubit ADAPT-VQE: Graph (a) Energy error convergence of the  $\text{H}_4$  molecule using the STO-3G basis set at  $r = 0.85\text{\AA}$  for several kinds of qubit pools according to their arrangement: full, full without Z, reduced without Z, XYXX, XXYX, XXXY, Random with first try (Random Try1), and second Try (Random Try2), two, four, and pool preserves symmetry (symmetry), see text. Graph(b) shows for each pool type the following estimated three properties: the number of CNOT gates (CNOT), the number of parameters/operators, the size of each pool (pool size).

do so using the BFGS optimizer in a similar VQE loop. Table 1 and Table 2 summarize the results obtained from calculations with each of the methods for LiH and  $\text{H}_6$ , respectively. We observe from Table 1 that fermionic ADAPT-VQE brings the most accurate values for the calculated energy by around two order of magnitudes compared with that of UCCSD and UCCGSD. A comparable accuracy between UCCSD and ADAPT-VQE occurs when a norm threshold  $10^{-2}$  is used in ADAPT-VQE (which could be also noticed in figure 2.b of<sup>41</sup>). This means that as the norm threshold decreases the ADAPT-VQE would bring better accuracy. Remarkably, the number of parameters/CNOTs (30/4624) is still small compared to UCCSD and UCCGSD even though the threshold considered is  $10^{-3}$ . Results shown in Table 2 demonstrate again that ADAPT-VQE yields the most accurate energy for the  $\text{H}_6$  molecule, by at least two orders of magnitude as compared to UCCGSD and UCCSD. Although UCCSD requires fewer number of parameters and CNOTs than with ADAPT-VQE, the latter brings better accuracy. This is

again due to the fact that we controlled the norm threshold to  $10^{-4}$ . A comparable accuracy between UCCSD and ADAPT-VQE in  $H_6$  occurs when a norm threshold  $10^{-1}$  is used in ADAPT-VQE as noticed in Figure 2(h) of reference<sup>41</sup>). It shows the fact that, at this level of threshold, ADAPT-VQE decrease the counts of CNOTs and parameters. UCCGSD energy appears in between UCCSD and ADAPT-VQE, but the number of CNOTs and parameters remain very high.

With those results, one can deduce that ADAPT-VQE brings more accurate results than UCCSD by several order of magnitudes, depending how the user can control the value of threshold, but the cost when using ADAPT-VQE with increased threshold is linked to the required high number of iterations and CNOTs. These latter increase increases with the number of qubits, which consequently leads to higher computational requirements in term of gradient computations. For UCCGSD (together with UCCSD), the analysis of numerical simulations applied to  $H_4$ ,  $H_2O$  and  $N_2$  were shown in reference<sup>49</sup>, illustrating the fact that although the UCCGSD ansatz yields very accurate results, the problem in using this method is linked to its high circuit depth. This is the opposite to the UCCSD case (or even k-UpCCGSD with at least  $k>2$ , see<sup>49</sup>).

## 6 | CONCLUSION AND FUTURE WORK

In this article, we discussed in details our newly introduced open source packages. They include the Open-VQE python package that enables to perform quantum chemistry computations based on the Quantum Machine Learning (QML) thanks to the newly introduced myQLM-fermion open source library that gather the key QLM resources that are important for quantum chemical developments. The Open-VQE/myQLM-fermion combined quantum simulator facilitates the implementation, tests and overall developments of variational quantum algorithms dedicated to quantum chemistry problems and provide state-of-the-art present quantum computing methods (see Table 3 which summarizes the GitHub links of the open-source quantum chemistry packages available to the community). Indeed we have shown that it enables users to construct modules in a few lines of python code using simple class structures related to the adaptive UCC family ansatze that we reviewed in the article. We also present how to easily implement efficient circuits related to fermionic and Qubit evolutions with the goal of reducing the CNOT gates. Using these modules, we generated benchmarks on a range of molecular computations from 4 to 22 qubits and obtained reliable results that appeared consistent with those previously obtained in reference literature (see<sup>35,98,99,70</sup> for the UCC and<sup>41,70,50,52</sup> for the ADAPT-VQE approaches). It is worth noting that technically the QLM machine is designed to simulate up to 41 Qubits on a large memory classical computer systems. Open-VQE is thus designed to simplify the researchers' work, providing with simple code modules thus facilitating the construction of new algorithms and ansatze.

Furthermore, Open-VQE benefits from the myQLM-fermion tools and allow to exchange/interact with other software quantum chemistry-oriented quantum computing packages (see Appendix B and Figure B2 ) enhancing the community capacity to work collectively and faster. We also intend to forge an efficient module that could merge the few keys tools required to run jobs on quantum computers such as IBM ones (as described in Appendix B. For example, Figure B1 ) show examples of simple code structure classes that involve the interoperability between different open source packages and QPUs.

We plan to extend further Open-VQE/myQLM-fermion tools towards reducing the quantum resources by building new modules describing functions that enable: (i) to tapper-off the number of qubits in VQE (alongside active space selection) through using penalty functions<sup>101</sup>, using point-group symmetry in small molecules<sup>102</sup> and in large molecules<sup>103</sup> and studying new functions that could preserve spatial symmetry of molecules (rotational and translational); (ii) to reduce the number of CNOT gates (alongside with MP2 guesses, efficient circuits, fermionic and qubit ADAPT-VQE) through implementing other adaptive algorithms such as permute qubit-VQE<sup>104</sup>.

Concerning chemical accuracy, we want to implement further methods to go beyond the chemically inspired UCC ansatze described in<sup>36</sup> (i.e. the implemented UCCSD, UCCGSD, spin-complement-gsd, k-UpCCGSD etc...). Equally we are interested in other types of UCC ansatze which involve higher-order correlation effects, such as MP3 or MP4, or triple excitation UCCSD(T) which could be important for strongly correlated systems and could improve further the accuracy as mentioned earlier<sup>49</sup>. We are also motivated to implement additional algorithms going beyond VQE, such as VQD (ADAPT-VQD) and QITE(ADAPT-QITE) that allow to determine excited state energies<sup>105,72,73,106,107</sup>.

Concerning optimization effects in the UCC family of methods, since we have demonstrated in the present work that some convergence problems might appear in ADAPT-VQE when targeting certain levels of accuracy, we want to make use of more efficient optimizer methods to overcome this problem. Of course, the practical use of VQE algorithms on present quantum computers will require to make Darwinian choices in link with qubit/operator counts and circuits depths restrictions: not all

algorithms will "make the cut" to the real quantum computing world. We believe that the present Open-VQE/myQLM-Fermion approach will help the community to study and design new accurate VQE algorithmic "champions" able to efficiently run on present and near-future NISQ quantum computers towards performing accurate quantum chemical computations on complex molecular systems.

**TABLE 1** LiH ( $r_{\text{Li-H}} = 1.45\text{\AA}$ ) in STO-3G basis set. Comparison between fixed-length ansatze: UCCSD and UCCGSD with fermionic ADAPT-VQE. In terms of number of parameters, CNOT-gates, Energy and Accuracy which is the absolute value of difference between Energy and FCI energy in Hartree (Ha).

Method	Parameters	CNOT-gates	Energy (Ha)	Error (Ha)	Computational time
UCCSD	44	6080	$-7.880973466$	$8.85 \times 10^{-6}$	1 hr, 11 min
UCCGSD	330	97280	$-7.880973130$	$9.18 \times 10^{-6}$	1 day, 12 hr
Fermionic ADAPT-VQE	30	4624	$-7.880982281$	$2.43 \times 10^{-8}$	2 hr, 43 min

**TABLE 2** Linear H<sub>6</sub> ( $r_{\text{H-H}} = 1.0\text{\AA}$ ) in STO-3G basis set. Comparison between fixed-length ansatze: UCCSD and UCCGSD with fermionic ADAPT-VQE. In terms of number of parameters, CNOT-gates, Energy and Accuracy the absolute value of difference between Energy and FCI energy.

Method	Parameters	CNOT-gates	Energy (Ha)	Error (Ha)	Computational time
UCCSD	54	8544	$-3.235451570$	$6.14 \times 10^{-4}$	3 hr, 10 min
UCCGSD	330	97280	$-3.2360518902$	$1.43 \times 10^{-5}$	5 days, 7hr
Fermionic ADAPT-VQE	130	21648	$-3.236065546$	$7.33 \times 10^{-7}$	7 day, 7 hr

**TABLE 3** Available implementations of individual approaches in a list of most recent open sources quantum chemistry simulation packages (Table referred from<sup>36</sup>) including Open-VQE and myQLM-fermion packages. Note: PNO-UpCCGSD stands for pair-natural orbitals-UpCCGSD and SPA for Separable Pair Approximation. The  $\times$  notation means that the method is NOT implemented in a given package.

package\ansatz	UCCSD	k-UpCCGSD	ADAPT	PNO-UpCCGSD	SPA	QPE
adapt-vqe	$\times$	$\times$	108	$\times$	$\times$	$\times$
TEQUILA	109	110	109	109,111	109,112	$\times$
PennyLane	113,114	115	113,116	$\times$	$\times$	$\times$
OpenFermion	117	$\times$	$\times$	$\times$	$\times$	$\times$
QEBA	118	118	119,118	$\times$	$\times$	$\times$
QFORTE	120	$\times$	120,121	$\times$	$\times$	120,122
Qiskit	123	$\times$	123	$\times$	$\times$	124
XACC	125	$\times$	$\times$	$\times$	$\times$	$\times$
QDK	126	$\times$	$\times$	$\times$	$\times$	126
InQuanto	127	$\times$	127	$\times$	$\times$	$\times$
Open-VQE/myQLM-fermion	53,54	53	53	$\times$	$\times$	54

## ACKNOWLEDGEMENTS

We are grateful to the European Union for the Horizon 2020 (H2020) research grant within the **NEIASIQC** project. This work has also received funding from the European Research Council (ERC) under the European Union's Horizon 2020 research and innovation program (grant agreement No 810367), project EMC2 (JPP, YM).

In addition, we would like to acknowledge all those who made this work possible: the TotalEnergies company for providing HPC resources.

Special thanks also to Diata Traore (LCT) for discussions on the classical quantum chemistry computations; to Baptiste Anselme Martin (Totalenergies) and Cesar Feniou (LCT) for helpful quantum computing discussions.

## References

1. Aspuru-Guzik A, Dutoi AD, Love PJ, Head-Gordon M. Simulated quantum computation of molecular energies. *Science* 2005; 309(5741): 1704–1707.
2. Bassman L, Urbanek M, Metcalf M, Carter J, Kemper AF, Jong dWA. Simulating quantum materials with digital quantum computers. *Quantum Science and Technology* 2021; 6(4): 043002.
3. Lehtola S, Tubman NM, Whaley KB, Head-Gordon M. Cluster decomposition of full configuration interaction wave functions: A tool for chemical interpretation of systems with strong correlation. *The Journal of chemical physics* 2017; 147(15): 154105.
4. Gan Z, Grant DJ, Harrison RJ, Dixon DA. The lowest energy states of the group-IIIA–group-VA heteronuclear diatomics: BN, BP, AlN, and AlP from full configuration interaction calculations. *The Journal of chemical physics* 2006; 125(12): 124311.
5. Vogiatzis KD, Ma D, Olsen J, Gagliardi L, De Jong WA. Pushing configuration-interaction to the limit: Towards massively parallel MCSCF calculations. *The Journal of chemical physics* 2017; 147(18): 184111.
6. Hohenberg P, Kohn W. Inhomogeneous electron gas. *Physical review* 1964; 136(3B): B864.
7. Kohn W, Sham LJ. Self-consistent equations including exchange and correlation effects. *Physical review* 1965; 140(4A): A1133.
8. Schütt O, VandeVondele J. Machine learning adaptive basis sets for efficient large scale density functional theory simulation. *Journal of chemical theory and computation* 2018; 14(8): 4168–4175.
9. Bartlett RJ, Kucharski SA, Noga J. Alternative coupled-cluster ansätze II. The unitary coupled-cluster method. *Chemical physics letters* 1989; 155(1): 133–140.
10. Kutzelnigg W. Error analysis and improvements of coupled-cluster theory. *Theoretica chimica acta* 1991; 80(4): 349–386.
11. Harrison RJ. Approximating full configuration interaction with selected configuration interaction and perturbation theory. *The Journal of chemical physics* 1991; 94(7): 5021–5031.
12. Olsen J, Jo/rsgensen P, Koch H, Balkova A, Bartlett RJ. Full configuration–interaction and state of the art correlation calculations on water in a valence double-zeta basis with polarization functions. *The Journal of chemical physics* 1996; 104(20): 8007–8015.
13. Peris G, Planelles J, Malrieu JP, Paldus J. Perturbatively selected CI as an optimal source for externally corrected CCSD. *The Journal of chemical physics* 1999; 110(24): 11708–11716.
14. Taube AG, Bartlett RJ. New perspectives on unitary coupled-cluster theory. *International journal of quantum chemistry* 2006; 106(15): 3393–3401.
15. Bartlett RJ, Musiał M. Coupled-cluster theory in quantum chemistry. *Reviews of Modern Physics* 2007; 79(1): 291.

16. Schriber JB, Evangelista FA. Communication: An adaptive configuration interaction approach for strongly correlated electrons with tunable accuracy. *The Journal of chemical physics* 2016; 144(16): 161106.
17. Nagy PR, Kállay M. Approaching the basis set limit of CCSD (T) energies for large molecules with local natural orbital coupled-cluster methods. *Journal of Chemical Theory and Computation* 2019; 15(10): 5275–5298.
18. Feynman RP. Simulating physics with computers. In: CRC Press. 2018 (pp. 133–153).
19. Benioff P. The computer as a physical system: A microscopic quantum mechanical Hamiltonian model of computers as represented by Turing machines. *Journal of statistical physics* 1980; 22(5): 563–591.
20. Reiher M, Wiebe N, Svore KM, Wecker D, Troyer M. Elucidating reaction mechanisms on quantum computers. *Proceedings of the national academy of sciences* 2017; 114(29): 7555–7560.
21. McArdle S, Endo S, Aspuru-Guzik A, Benjamin SC, Yuan X. Quantum computational chemistry. *Reviews of Modern Physics* 2020; 92(1): 015003.
22. Cao Y, Romero J, Olson JP, et al. Quantum chemistry in the age of quantum computing. *Chemical reviews* 2019; 119(19): 10856–10915.
23. Bauer B, Bravyi S, Motta M, Chan GKL. Quantum algorithms for quantum chemistry and quantum materials science. *Chemical Reviews* 2020; 120(22): 12685–12717.
24. Yeter-Aydeniz K, Gard BT, Jakowski J, et al. Benchmarking quantum chemistry computations with variational, imaginary time evolution, and Krylov space solver algorithms. *Advanced Quantum Technologies* 2021; 4(7): 2100012.
25. Whitfield JD, Biamonte J, Aspuru-Guzik A. Simulation of electronic structure Hamiltonians using quantum computers. *Molecular Physics* 2011; 109(5): 735–750.
26. Preskill J. Quantum computing in the NISQ era and beyond. *Quantum* 2018; 2: 79.
27. Elfving VE, Broer BW, Webber M, et al. How will quantum computers provide an industrially relevant computational advantage in quantum chemistry?. *arXiv preprint arXiv:2009.12472* 2020.
28. Bharti K, Cervera-Lierta A, Kyaw TH, et al. Noisy intermediate-scale quantum (NISQ) algorithms. *arXiv preprint arXiv:2101.08448* 2021.
29. Peruzzo A, McClean J, Shadbolt P, et al. A variational eigenvalue solver on a photonic quantum processor. *Nature communications* 2014; 5(1): 1–7.
30. McClean JR, Romero J, Babbush R, Aspuru-Guzik A. The theory of variational hybrid quantum-classical algorithms. *New Journal of Physics* 2016; 18(2): 023023.
31. Cerezo M, Arrasmith A, Babbush R, et al. Variational quantum algorithms. *Nature Reviews Physics* 2021; 3(9): 625–644.
32. Quantum GA, Collaborators\*†, Arute F, et al. Hartree-Fock on a superconducting qubit quantum computer. *Science* 2020; 369(6507): 1084–1089.
33. Kandala A, Mezzacapo A, Temme K, et al. Hardware-efficient variational quantum eigensolver for small molecules and quantum magnets. *Nature* 2017; 549(7671): 242–246.
34. Hempel C, Maier C, Romero J, et al. Quantum chemistry calculations on a trapped-ion quantum simulator. *Physical Review X* 2018; 8(3): 031022.
35. Romero J, Babbush R, McClean JR, Hempel C, Love PJ, Aspuru-Guzik A. Strategies for quantum computing molecular energies using the unitary coupled cluster ansatz. *Quantum Science and Technology* 2018; 4(1): 014008.
36. Anand A, Schleich P, Alperin-Lea S, et al. A quantum computing view on unitary coupled cluster theory. *Chemical Society Reviews* 2022.

37. Gard BT, Zhu L, Barron GS, Mayhall NJ, Economou SE, Barnes E. Efficient symmetry-preserving state preparation circuits for the variational quantum eigensolver algorithm. *npj Quantum Information* 2020; 6(1): 1–9.
38. Ryabinkin IG, Yen TC, Genin SN, Izmaylov AF. Qubit coupled cluster method: a systematic approach to quantum chemistry on a quantum computer. *Journal of chemical theory and computation* 2018; 14(12): 6317–6326.
39. Kim IH, Swingle B. Robust entanglement renormalization on a noisy quantum computer. *arXiv preprint arXiv:1711.07500* 2017.
40. Wecker D, Hastings MB, Troyer M. Progress towards practical quantum variational algorithms. *Physical Review A* 2015; 92(4): 042303.
41. Grimsley HR, Economou SE, Barnes E, Mayhall NJ. An adaptive variational algorithm for exact molecular simulations on a quantum computer. *Nature communications* 2019; 10(1): 1–9.
42. McClean JR, Kimchi-Schwartz ME, Carter J, De Jong WA. Hybrid quantum-classical hierarchy for mitigation of decoherence and determination of excited states. *Physical Review A* 2017; 95(4): 042308.
43. myQLM package. <https://myqlm.github.io/> ; .
44. Interoperability with myQLM. [https://myqlm.github.io/myqlm\\_specific/interoperability.html](https://myqlm.github.io/myqlm_specific/interoperability.html) ; .
45. Wille R, Van Meter R, Naveh Y. IBM’s Qiskit tool chain: Working with and developing for real quantum computers. In: IEEE. ; 2019: 1234–1240.
46. Developers C. Cirq. <https://github.com/quantumlib/Cirq/graphs/contributors>; 2021. See full list of authors on Github: <https://github.com/quantumlib/Cirq/graphs/contributors>
47. Smith RS, Curtis MJ, Zeng WJ. A practical quantum instruction set architecture. *arXiv preprint arXiv:1608.03355* 2016.
48. Nooijen M. Can the eigenstates of a many-body hamiltonian be represented exactly using a general two-body cluster expansion?. *Physical review letters* 2000; 84(10): 2108.
49. Lee J, Huggins WJ, Head-Gordon M, Whaley KB. Generalized unitary coupled cluster wave functions for quantum computation. *Journal of chemical theory and computation* 2018; 15(1): 311–324.
50. Tang HL, Shkolnikov V, Barron GS, et al. qubit-adapt-vqe: An adaptive algorithm for constructing hardware-efficient ansätze on a quantum processor. *PRX Quantum* 2021; 2(2): 020310.
51. Xia R, Kais S. Qubit coupled cluster singles and doubles variational quantum eigensolver ansatz for electronic structure calculations. *Quantum Science and Technology* 2020; 6(1): 015001.
52. Shkolnikov V, Mayhall NJ, Economou SE, Barnes E. Avoiding symmetry roadblocks and minimizing the measurement overhead of adaptive variational quantum eigensolvers. *arXiv preprint arXiv:2109.05340* 2021.
53. Open-VQE package. <https://github.com/OpenVQE/OpenVQE.git><https://openvqe.github.io/OpenVQE/>; .
54. myqlm-fermion. <https://github.com/myQLM/myqlm-fermion><https://myqlm.github.io/qat-fermion.html> ; .
55. Barreiro JT, Müller M, Schindler P, et al. An open-system quantum simulator with trapped ions. *Nature* 2011; 470(7335): 486–491.
56. Fradkin E. Jordan-Wigner transformation for quantum-spin systems in two dimensions and fractional statistics. *Physical review letters* 1989; 63(3): 322.
57. Virtanen P, Gommers R, Oliphant TE, et al. SciPy 1.0: Fundamental Algorithms for Scientific Computing in Python. *Nature Methods* 2020; 17: 261–272. doi: 10.1038/s41592-019-0686-2

58. Čížek J. On the correlation problem in atomic and molecular systems. Calculation of wavefunction components in Ursell-type expansion using quantum-field theoretical methods. *The Journal of Chemical Physics* 1966; 45(11): 4256–4266.
59. Cizek J, Paldus J. Coupled cluster approach. *Physica Scripta* 1980; 21(3-4): 251.
60. Yung MH, Casanova J, Mezzacapo A, et al. From transistor to trapped-ion computers for quantum chemistry. *Scientific reports* 2014; 4(1): 1–7.
61. Taube AG, Bartlett RJ. New perspectives on unitary coupled-cluster theory. *International journal of quantum chemistry* 2006; 106(15): 3393–3401.
62. Evangelista FA, Chan GKL, Scuseria GE. Exact parameterization of fermionic wave functions via unitary coupled cluster theory. *The Journal of chemical physics* 2019; 151(24): 244112.
63. Grimsley HR, Claudino D, Economou SE, Barnes E, Mayhall NJ. Is the trotterized uccsd ansatz chemically well-defined?. *Journal of chemical theory and computation* 2019; 16(1): 1–6.
64. Hatano N, Suzuki M. Finding exponential product formulas of higher orders. In: Springer. 2005 (pp. 37–68).
65. Göbel T. On the physics of Trotterization. *Leiden University Student Repository* 2020.
66. Barkoutsos PK, Gonthier JF, Sokolov I, et al. Quantum algorithms for electronic structure calculations: Particle-hole Hamiltonian and optimized wave-function expansions. *Physical Review A* 2018; 98(2): 022322.
67. Yordanov YS, Barnes CH. Implementation of a general single-qubit positive operator-valued measure on a circuit-based quantum computer. *Physical Review A* 2019; 100(6): 062317.
68. Yordanov YS, Arvidsson-Shukur DR, Barnes CH. Efficient quantum circuits for quantum computational chemistry. *Physical Review A* 2020; 102(6): 062612.
69. Yordanov YS, Armaos V, Barnes CH, Arvidsson-Shukur DR. Qubit-excitation-based adaptive variational quantum eigensolver. *Communications Physics* 2021; 4(1): 1–11.
70. Yordanov Y. *Quantum computational chemistry methods for early-stage quantum computers*. PhD thesis. University of Cambridge, Cambridge, UK; 2021.
71. Huggins WJ, Lee J, Baek U, O’Gorman B, Whaley KB. A non-orthogonal variational quantum eigensolver. *New Journal of Physics* 2020; 22(7): 073009.
72. Greene-Diniz G, Muñoz Ramo D. Generalized unitary coupled cluster excitations for multireference molecular states optimized by the variational quantum eigensolver. *International Journal of Quantum Chemistry* 2021; 121(4): e26352.
73. Chan HHS, Fitzpatrick N, Segarra-Martí J, Bearpark MJ, Tew DP. Molecular excited state calculations with adaptive wavefunctions on a quantum eigensolver emulation: reducing circuit depth and separating spin states. *Physical Chemistry Chemical Physics* 2021; 23(46): 26438–26450.
74. Rattew AG, Hu S, Pistoia M, Chen CFR, Wood S. A domain-agnostic, noise-resistant evolutionary variational quantum eigensolver for hardware-efficient optimization in the Hilbert space. *DeepAI* 2019.
75. Ryabinkin IG, Lang RA, Genin SN, Izmaylov AF. Iterative qubit coupled cluster approach with efficient screening of generators. *Journal of chemical theory and computation* 2020; 16(2): 1055–1063.
76. Lang RA, Ryabinkin IG, Izmaylov AF. Unitary transformation of the electronic hamiltonian with an exact quadratic truncation of the baker-campbell-hausdorff expansion. *Journal of Chemical Theory and Computation* 2020; 17(1): 66–78.
77. Sim S, Romero J, Gonthier JF, Kunitsa AA. Adaptive pruning-based optimization of parameterized quantum circuits. *Quantum Science and Technology* 2021; 6(2): 025019.
78. Liu J, Li Z, Yang J. An efficient adaptive variational quantum solver of the Schrödinger equation based on reduced density matrices. *The Journal of chemical physics* 2021; 154(24): 244112.

79. Quantum Learning Machine. <https://atos.net/en/solutions/quantum-learning-machine> ATOS Quantum Learning Machine; .

80. Martiel S, Brugi  re dTG. Architecture aware compilation of quantum circuits via lazy synthesis. *Quantum* 2020. doi: 10.48550/ARXIV.2012.09663

81. De Brugi  re TG, Baboulin M, Valiron B, Martiel S, Allouche C. Gaussian Elimination versus Greedy Methods for the Synthesis of Linear Reversible Circuits. *ACM Transactions on Quantum Computing* 2021; 2(3). doi: 10.1145/3474226

82. Vandaele V, Martiel S, Brugi  re G. dT. Phase polynomials synthesis algorithms for NISQ architectures and beyond. *Quantum Science and Technology* 2022.

83. Brugi  re TGd, Baboulin M, Valiron B, Martiel S, Allouche C. Reducing the Depth of Linear Reversible Quantum Circuits. *IEEE Transactions on Quantum Engineering* 2021; 2: 1-22. doi: 10.1109/TQE.2021.3091648

84. Brugi  re dTG, Baboulin M, Valiron B, Martiel S, Allouche C. Decoding techniques applied to the compilation of CNOT circuits for NISQ architectures. *ScienceDirect* 2022; 214(February 2022): 1–31. doi: 10.1016/j.scico.2021.102726

85. Vidal G. Efficient Classical Simulation of Slightly Entangled Quantum Computations. *Phys. Rev. Lett.* 2003; 91: 147902. doi: 10.1103/PhysRevLett.91.147902

86. Rudiak-Gould B. The sum-over-histories formulation of quantum computing. *arXiv preprint quant-ph/0607151* 2006.

87. Miller DM, Thornton MA. QMDD: A decision diagram structure for reversible and quantum circuits. In: IEEE. ; 2006: 30–30.

88. Loos PF, Damour Y, Scemama A. The performance of CIPSI on the ground state electronic energy of benzene. *The Journal of Chemical Physics* 2020; 153(17): 176101.

89. Garniron Y. *Development and parallel implementation of selected configuration interaction methods*. PhD thesis. Universit   de Toulouse, Toulouse, France; 2019

90. Quantum Package: a programming environment for wave function methods. <https://github.com/QuantumPackage/qp2>, <https://github.com/quantumlib/Cirq/graphs/contributors>; .

91. Gunnarsson O, Lundqvist BI. Exchange and correlation in atoms, molecules, and solids by the spin-density-functional formalism. *Physical Review B* 1976; 13(10): 4274.

92. Running Gaussian. <https://gaussian.com/running/>; .

93. Garniron Y, Applencourt T, Gasperich K, et al. Quantum Package 2.0: An Open-Source Determinant-Driven Suite of Programs. *Journal of Chemical Theory and Computation* 2019; 15(6): 3591-3609. PMID: 31082265doi: 10.1021/acs.jctc.9b00176

94. Lovas F, Tiemann E, Coursey J, et al. Diatomic Spectral Database. <https://www.nist.gov/pml/diatomic-spectral-database> Diatomic spectral database; 2003.

95. Herzberg G. *Electronic spectra and electronic structure of polyatomic molecules*. New York : Van Nostrand . 1966.

96. Huber KP. *Molecular spectra and molecular structure: IV. Constants of diatomic molecules*. Springer Science & Business Media . 2013.

97. al. eRDJ. NIST computational chemistry comparison and benchmark database, NIST standard reference database number 101 release 21. <https://cccbdb.nist.gov/>; 2020.

98. Harsha G, Shiozaki T, Scuseria GE. On the difference between variational and unitary coupled cluster theories. *The Journal of chemical physics* 2018; 148(4): 044107.

99. K  hn M, Zanker S, Deglmann P, Marthaler M, Wei   H. Accuracy and resource estimations for quantum chemistry on a near-term quantum computer. *Journal of chemical theory and computation* 2019; 15(9): 4764–4780.

100. Carrazza S, Efthymiou S, Lazzarin M, Pasquale A. An open-source modular framework for quantum computing. *arXiv preprint arXiv:2202.07017* 2022.
101. Kuroiwa K, Nakagawa YO. Penalty methods for a variational quantum eigensolver. *Physical Review Research* 2021; 3(1): 013197.
102. Setia K, Chen R, Rice JE, Mezzacapo A, Pistoia M, Whitfield JD. Reducing qubit requirements for quantum simulations using molecular point group symmetries. *Journal of Chemical Theory and Computation* 2020; 16(10): 6091–6097.
103. Cao C, Hu J, Zhang W, et al. Towards a Larger Molecular Simulation on the Quantum Computer: Up to 28 Qubits Systems Accelerated by Point Group Symmetry. *arXiv preprint arXiv:2109.02110* 2021.
104. Tkachenko NV, Sud J, Zhang Y, et al. Correlation-informed permutation of qubits for reducing ansatz depth in the variational quantum eigensolver. *PRX Quantum* 2021; 2(2): 020337.
105. Ollitrault PJ, Kandala A, Chen CF, et al. Quantum equation of motion for computing molecular excitation energies on a noisy quantum processor. *Physical Review Research* 2020; 2(4): 043140.
106. Ville JL, Morvan A, Hashim A, et al. Leveraging randomized compiling for the QITE algorithm. *arXiv preprint arXiv:2104.08785* 2021.
107. Kamakari H, Sun SN, Motta M, Minnich AJ. Digital quantum simulation of open quantum systems using quantum imaginary-time evolution. *PRX Quantum* 2022; 3(1): 010320.
108. ADAPT package. <https://github.com/mayhallgroup/adapt-vqe.git>; .
109. Kottmann JS, Alperin-Lea S, Tamayo-Mendoza T, et al. Tequila: A platform for rapid development of quantum algorithms. *Quantum Science and Technology* 2021; 6(2): 024009.
110. Pair-natural orbitals in tequila package. <https://github.com/aspuru-guzik-group/tequila>; .
111. Kottmann JS, Schleich P, Tamayo-Mendoza T, Aspuru-Guzik A. Reducing qubit requirements while maintaining numerical precision for the variational quantum eigensolver: A basis-set-free approach. *The Journal of Physical Chemistry Letters* 2021; 12(1): 663–673.
112. Kottmann JS, Aspuru-Guzik A. Optimized low-depth quantum circuits for molecular electronic structure using a separable-pair approximation. *Physical Review A* 2022; 105(3): 032449.
113. Bergholm V, Izaac J, Schuld M, et al. Pennylane: Automatic differentiation of hybrid quantum-classical computations. *arXiv preprint arXiv:1811.04968* 2018.
114. Arrazola JM, Di Matteo O, Quesada N, Jahangiri S, Delgado A, Killoran N. Universal quantum circuits for quantum chemistry. *arXiv preprint arXiv:2106.13839* 2021.
115. PennyLaneAI package. <https://github.com/PennyLaneAI/pennylane.git>; .
116. Delgado A, Arrazola JM, Jahangiri S, et al. Variational quantum algorithm for molecular geometry optimization. *Physical Review A* 2021; 104(5): 052402.
117. McClean JR, Rubin NC, Sung KJ, et al. OpenFermion: the electronic structure package for quantum computers. *Quantum Science and Technology* 2020; 5(3): 034014.
118. QEBA package. <https://github.com/hanschanhs/QEBA.git>; .
119. Chan HHS, Fitzpatrick N, Segarra-Martí J, Bearpark MJ, Tew DP. Molecular excited state calculations with adaptive wavefunctions on a quantum eigensolver emulation: reducing circuit depth and separating spin states. *Physical Chemistry Chemical Physics* 2021; 23(46): 26438–26450.

120. Stair NH, Evangelista FA. Qforte: an efficient state simulator and quantum algorithms library for molecular electronic structure. *arXiv preprint arXiv:2108.04413* 2021.
121. Stair NH, Evangelista FA. Simulating many-body systems with a projective quantum eigensolver. *PRX Quantum* 2021; 2(3): 030301.
122. Stair NH, Huang R, Evangelista FA. A multireference quantum krylov algorithm for strongly correlated electrons. *Journal of chemical theory and computation* 2020; 16(4): 2236–2245.
123. Aleksandrowicz G, Alexander T, Barkoutsos P, et al. Qiskit: An Open-source Framework for Quantum Computing. <https://doi.org/10.5281/zenodo.2562111>; 2019
124. Quantum phase estimation algorithm in Qiskit package. <https://qiskit.org/textbook/ch-algorithms/quantum-phase-estimation.html><https://qiskit.org/textbook/ch-algorithms/quantum-phase-estimation.html> .
125. McCaskey AJ, Lyakh DI, Dumitrescu EF, Powers SS, Humble TS. XACC: a system-level software infrastructure for heterogeneous quantum–classical computing. *Quantum Science and Technology* 2020; 5(2): 024002.
126. Quantum Development Kit. <https://github.com/microsoft/quantum.git>; .
127. InQuanto package. <https://medium.com/cambridge-quantum-computing/introduction-to-the-inquanto-computational-chemistry-platform-for-quantum-computers>;
- .

**How to cite this article:** M. Haidar, M. J. Rančić, T. Ayral, Y. Maday, and J-P. Piquemal (2022), Open Source Variational Quantum Eigensolver Extension of the Quantum Learning Machine (QLM) for Quantum Chemistry, , .

## APPENDIX

### A REVIEW: SPIN-COMPLEMENT GENERALIZED SINGLET AND DOUBLET EXCITATIONS

#### Spin-complement pair:

is a method that involves excitations that can preserve spin-symmetry for neutral closed-shell molecules (i.e number of  $\alpha$  electrons = number of  $\beta$  electrons). These excitations restrict the spin-symmetry of the UCC wavefunction Hilbert space into a smaller Hilbert space with the desired eigenstate. In order to satisfy such spin-symmetry, only the excitations that keep balance between  $\alpha$  and  $\beta$  electrons should be implemented as follows:

$$\tau_1 = c_{p_\alpha}^\dagger c_{q_\alpha} + c_{p_\beta}^\dagger c_{q_\beta} - h.c. \quad (A1)$$

$$\begin{aligned} \tau_{2,A} &= c_{r_\alpha}^\dagger c_{s_\alpha} c_{p_\alpha}^\dagger c_{q_\alpha} + c_{r_\beta}^\dagger c_{s_\beta} c_{p_\beta}^\dagger c_{q_\beta} - h.c. \\ \tau_{2,B} &= c_{r_\alpha}^\dagger c_{s_\beta} c_{p_\alpha}^\dagger c_{q_\beta} + c_{r_\beta}^\dagger c_{s_\alpha} c_{p_\beta}^\dagger c_{q_\alpha} - h.c. \\ \tau_{2,C} &= c_{r_\alpha}^\dagger c_{s_\beta} c_{p_\beta}^\dagger c_{q_\alpha} + c_{r_\beta}^\dagger c_{s_\alpha} c_{p_\alpha}^\dagger c_{q_\beta} - h.c. \end{aligned} \quad (A2)$$

This type of fermionic excitations is called spin-complemented pair: as is seen above in (Eqs. A1 and Eqs. A2), for each unitary operator acting on some spin orbitals, there is an added parallel unitary operator that acts on the opposite-spin orbitals. Spin-complemented pair excitations, have been used within the Fermionic ADAPT-VQE<sup>41</sup>, which is used in this article when fermionic ADAPT-VQE is implemented.

## B INTEROPERABILITY OF OPEN-SOURCE PACKAGES WITH MYQLM

One of the main advantages of myQLM library as mentioned in section 3 is to allow the developers and researchers to access through it to other quantum programming environments such as Qiskit, projectQ, pyQuil, Cirq etc. We want to shed light in this section about the interoperability of myQLM circuit to other circuits corresponding to those packages. myQLM library provides binders to connect with the other Python-based quantum frameworks. The role of these binders is to: (i) translate myQLM circuits into a format defined in another quantum framework and vice-versa. (ii) execute a job using a QPU defined in another quantum framework directly in myQLM and vice-versa. This is helpful to any problem in quantum computing.

When it comes to our domain of treating quantum chemistry problems using variational quantum algorithms it is important to use myQLM tools to translate a defined wavefunction represented by a QLM circuit into Qiskit, Cirq, PyQuil etc. This bridges the gap between the chemists who work in myQLM softwares and those who work on the other packages. This allows them to validate their calculations and their codes. This exchange between packages works easily for the user by just using few lines of codes developed by myQLM package.

It is interesting to realize that as we develop our VQE algorithms basing them on myQLM-fermion tools, we will certainly need the myQLM interoperability binders to interact with the other packages. This provides tests to our developed algorithms to compare them with those implemented in other packages.

Additionally, using this interoperability, can facilitate for the user the execution of a circuit in a real quantum device as shown in the figure below For example to describe the QLM-Qiskit circuits switching using myQLM keys, we provide a simple example



**FIGURE B1** myQLM keys: running on IBM quantum computer

related to an advanced VQE algorithm which we developed in Open-VQE described in section 4. This hopefully will make the image of myQLM interoperability clearer to the reader. As explained in section 2.4, qubit ADAPT-VQE is based on pool of excitations consisting of Pauli strings that can be added adaptively step by step to construct the final ansatz. Suppose our pool consist of the  $YXYY$  strings. Then mapping the exponential of each of these strings associated with their parameters into a circuit

can be done typically by using CNOTstair case method. myQLM-fermion tools can help to slice this exponential to construct this circuit, which we name it here "YXYYQLM", this construction is shown in Figure B2 . By using the keys of myQLM listed in the same Figure, the user can switch between YXYYQLM and YXYYQiskit immediately.

We can also use other myQLM tools not only to switch QLM and Qiskit circuits but also to connect between myQLM QPU and Qiskit Backend when we want to execute a job and obtain an estimated energy. With myQLM<sup>44</sup> one can simply use a circuit to test it in a real IBM computer by doing the following few steps presented in Figure B1 : (i) First to declare your IBM token, (ii) second to wrap a Qiskit backend in a QPU, (iii) third to use job class in order to send the circuit to a QPU then just submit the job to IBM to obtain the results. Further details about the code documentation of these tools and binders are found in myQLM website<sup>43</sup>.

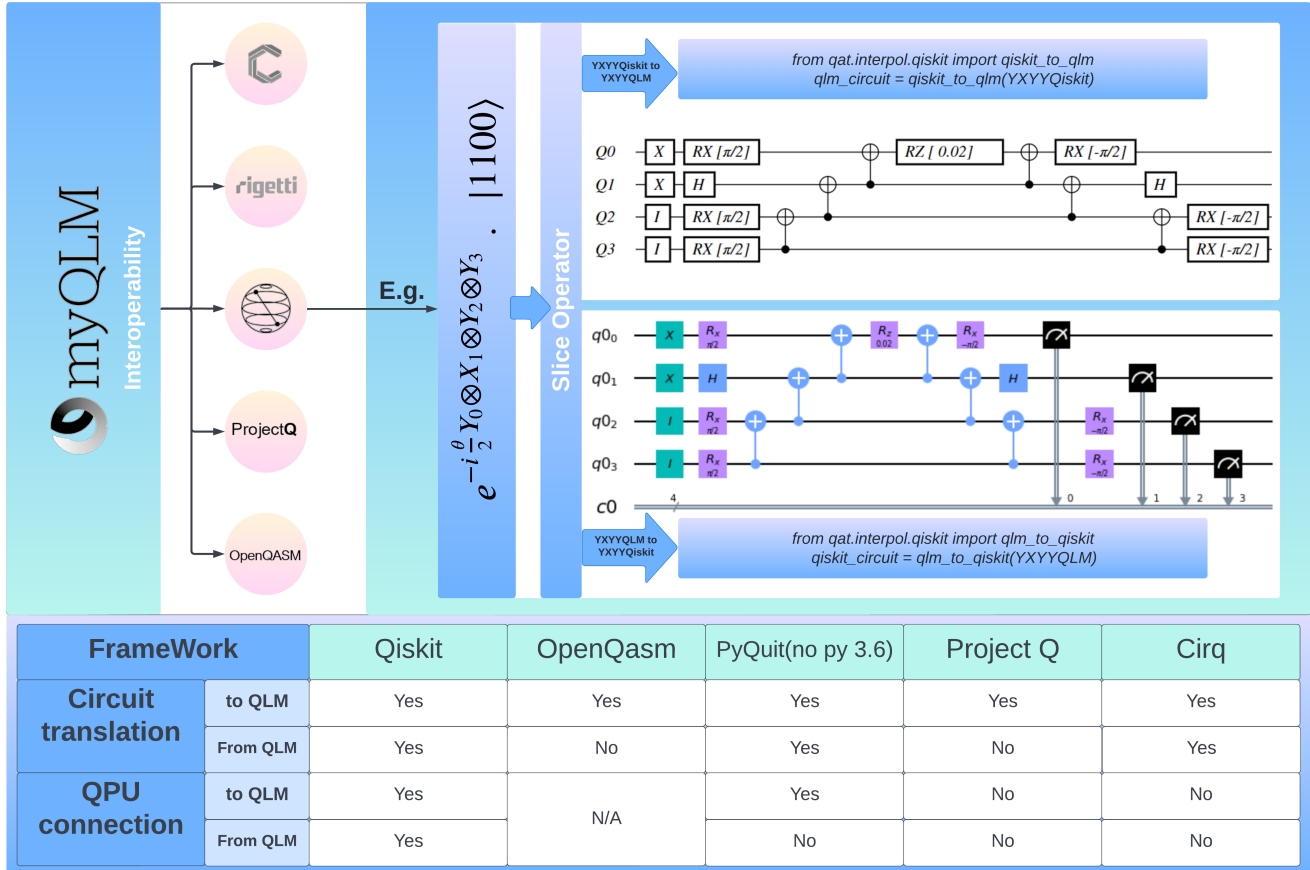
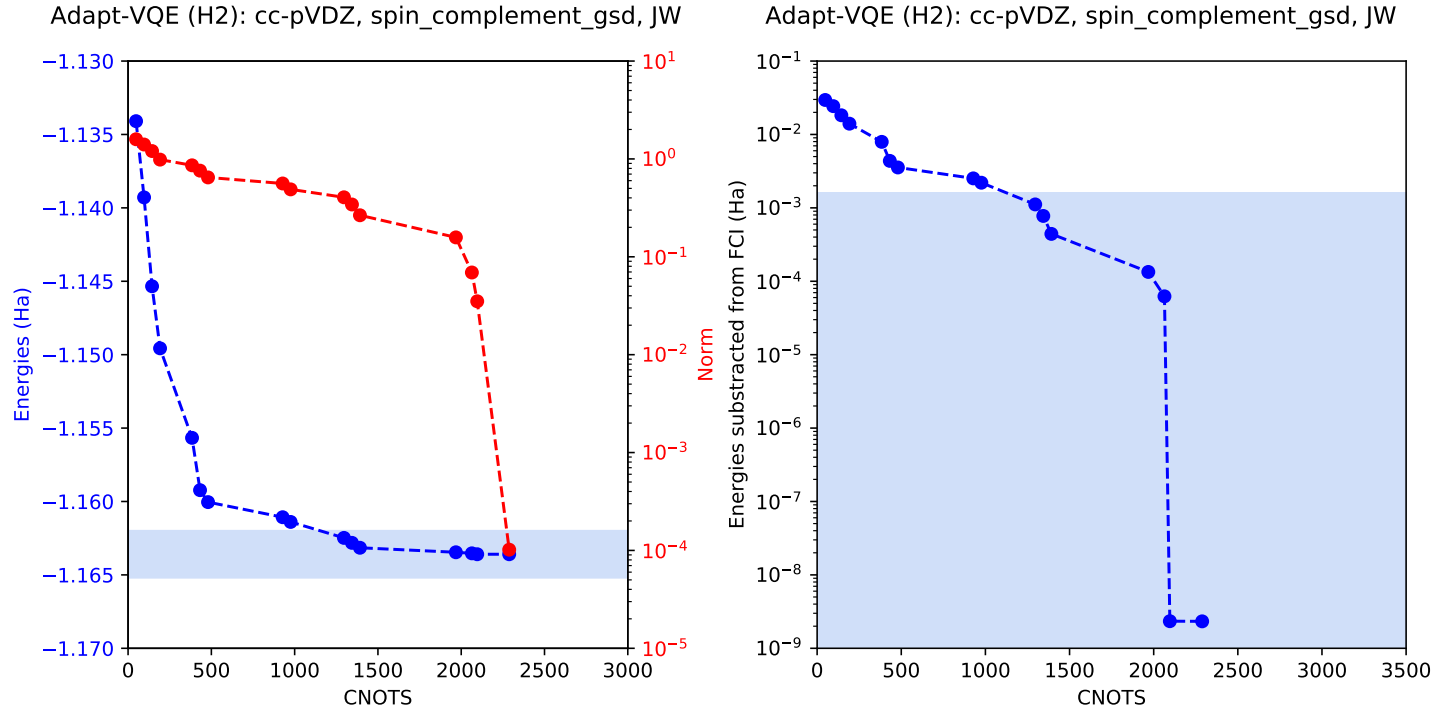


**FIGURE B2** Interoperability packages with myQLM. YXYYQLM (top circuit) and YXYY (bottom circuit). These circuits consists of 4 qubits that represents  $e^{Y_0 \otimes X_1 \otimes Y_2 \otimes Y_3} |1100\rangle$  with  $\theta$  is equal to 0.01.

## C FERMIONIC ADAPT-VQE-EXAMPLE: ENERGY VERSUS THE NORM THRESHOLD IN H<sub>2</sub> MOLECULE IN CC-PVDZ BASIS SET



**(a)** Energy (Ha), Norm thresholds (red) as a function of CNOT gates **(b)** Error for the ground state energy given in subfigure(a) w.r.t FCI(cc-pVDZ) basis set as a function of CNOT gates

**FIGURE C3** Fermionic ADAPT VQE simulations in H<sub>2</sub> molecule (20 qubits) in cc-pVDZ basis set. Iterations were stopped based on a given norm threshold condition (which stops here at  $10^{-4}$ ). The blue area represent the chemical accuracy.